DMD Fast Forward. Published on July 22, 2014 as DOI: 10.1124/dmd.114.058222
This article has not been copyedited and formatted. The final version may differ from this version.

DMD #58222

Metabolism of Diosbulbin B *in vitro* and *in vivo* in Rats: Formation of Reactive Metabolites and Human Enzymes Involved

Baohua Yang, Wei Liu, Kaixian Chen, Zhengtao Wang, Changhong Wang

The MOE Key Laboratory for Standardization of Chinese Medicines and The SATCM Key Laboratory for New Resources and Quality Evaluation of Chinese Medicines; Institute of Chinese Materia Medica, Shanghai University of Traditional Chinese Medicine, 1200 Cailun Road, Shanghai 201210, China. (BY, WL, KC, ZW and CW)

Shanghai R&D Centre for Standardization of Chinese Medicines, 199 Guoshoujing Road, Shanghai 201210, China. (KC, ZW and CW)

Running Title:

Reactive Metabolites of Diosbulbin B and Human Enzymes Involved

Corresponding authors:

Changhong Wang, E-mail address: wchcxm@hotmail.com; Zhengtao Wang, Email address: wangzht@hotmail.com; Phone: + 86 21 51322511; Fax: + 86 21 51322519

Number of pages: 35

Number of tables: 4

Number of figures: 12

Number of references: 34

Number of words in the abstract: 231

Number of words in the introduction: 520

Number of words in the discussions: 1181

Abbreviations:

CYP450: Cytochrome P450; COSY: Correlation spectroscopy; DB: Diosbulbin B; DMDO: Dimethyldioxirane; DMSO: Dimethyl sulfoxide; GSH: glutathione; HLM: Human liver microsomes; HMBC: Heteronuclear multiple bond correlation; HPLC: High-performance liquid chromatography; HSQC: Heteronuclear single quantum coherence; IS: Internal standard; MGCD: mono-GSH conjugates of DB; MRM: Multiple reaction mode; MS: Mass spectrometry; MS/MS: Mass spectrometry tandem mass spectrometry; NOESY: Nuclear Overhauser effect spectroscopy; RLM: Rat liver microsomes; RAF: Relative activity factor; TIC: Total ion current; UPLC-MS: Ultra-performance liquid chromatography tandem mass spectrometry.

DMD Fast Forward. Published on July 22, 2014 as DOI: 10.1124/dmd.114.058222
This article has not been copyedited and formatted. The final version may differ from this version.

Abstract

Diosbulbin B (DB), a major constituent of the furano-norditerpenes in *Dioscorea bulbifera* Linn, exhibits potential antineoplasmic activity and hepatotoxicity. The metabolism and reactive metabolites of DB *in vitro* (with human and animal liver microsomes) and *in vivo* in rats were investigated. The human enzymes involved in DB metabolism were identified. DB was first catalyzed into reactive metabolites of 2-butene-1,4-dial derivatives dependent on NADPH and then trapped by Tris base or oxidized to hemiacetal lactones (M12 and M13) in microsomal incubations. Tris base was used as buffer constituent and as trapping agent for aldehyde. Methoxylamine and glutathione (GSH) were also used as trapping agents. DB metabolism *in vivo* in rats after oral administration was consistent with that *in vitro*. The structures of M12 and M13, as well as mono-GSH conjugates of DB, M31, were confirmed by nuclear magnetic resonance spectroscopy of the chemically synthesized products. The bioactivation enzymes of DB were identified as CYP3A4/5, 2C9, and 2C19. CYP3A4 was found to be the primary enzyme using human recombinant cytochrome P450 (CYP450) enzymes, specific inhibitory studies, and a relative activity factor approach for pooled human liver microsomes. Michaelis-Menten constants K_m and V_{max} were determined by the formation of M31. The reactive metabolites may be related to the hepatotoxicity of DB. The gender difference in CYP3A expression in mice and rats contributed to the gender-related liver injury and pharmacokinetics in mice and rats, respectively.

DMD Fast Forward. Published on July 22, 2014 as DOI: 10.1124/dmd.114.058222
This article has not been copyedited and formatted. The final version may differ from this version.

Introduction

Diosbulbin B (DB) is a major constituent of the furano-norditerpenes in *Dioscorea bulbifera* Linn, which has been used in traditional Chinese medicine as remedy for sore throat, struma, and tumor (Zhang et al., 2008). Severe liver injuries, including liver failures, and even death had been reported in patients who took *D. bulbifera* for more than eight consecutive days (Niu and Chen, 1994). Many diosbulbins, which include diosbulbin A - H (Kawasaki et al., 1968; Ida et al., 1978), diosbulbin I - J (Wang et al., 2009), and diosbulbin K - M, have been separated and identified from *D. Bulbifera* (Liu et al., 2010). DB has been confirmed as one of the main hepatotoxic constituents in *D. bulbifera*. This compound also causes gender-related liver injury in mice (Wang et al., 2010) as well as gender-related pharmacokinetic behavior in rats (Yang et al., 2013). DB also exhibits remarkable antitumor activity in S180 cell-bearing mice (Wang et al., 2012; Komori, 1997), but no activity in tumor cell line *in vitro* (Komori, 1997). These data implies that DB metabolism plays an important role in the pharmacological activity and hepatotoxicity of DB *in vivo*.

Xenobiotics are usually converted to chemicals that can be more readily eliminated from the body by metabolic biotransformation once they enter the body. Xenobiotics metabolites may be classified into the following broad classes according to their pharmacological properties: (a) inactive metabolites, which possess no pharmacological activity; (b) active metabolites, which may have pharmacological properties of lower, equal, or greater magnitude than their parent compounds; and (c) reactive metabolites that can covalently react with and alter the functional macromolecular structure of endogenous targets *in vivo*, resulting in unwanted toxic effects (Njuguna et al., 2012). For example, teucrin A, a *neo*-clerodane diterpene in germander (*Teucrium chamaedrys*), is a structural analog of DB. Oral administration of teucrin A or extract from germander could induce significant hepatic necrosis in mice, which has been attributed to the metabolic activation of furan moiety to 1,4-enedials reactive metabolites (Druckova and Marnett, 2006).

DMD Fast Forward. Published on July 22, 2014 as DOI: 10.1124/dmd.114.058222
This article has not been copyedited and formatted. The final version may differ from this version.

Available information on DB metabolism is insufficient. Thus, in the present study, DB metabolism *in vitro* was investigated using liver microsomes from human and animals, such as rat, mice, rabbit, and guinea pig, using ultra-performance liquid chromatography tandem mass spectrometry (UPLC-MS). DB metabolites in urine, feces, bile, and plasma of rats after oral administration of DB were also identified. GSH and methoxylamine were used as trapping agents in the incubation *in vitro* once the reactive metabolites were distinguished by the formation of Tris base conjugates of DB. To confirm the structures of the reactive metabolites, mono-GSH conjugates of DB (MGCD) were chemically synthesized, purified by semi-preparative high-performance liquid chromatography (HPLC) and identified by nuclear magnetic resonance (NMR) spectroscopy. The bioactivation enzymes of DB were identified using human recombinant CYP450 enzymes. Michaelis-Menten constants K_m and V_{max} were estimated by the formation of MGCD. Moreover, the importance of CYP450 isoforms for the bioactivation of DB were determined using specific inhibitory studies and relative activity factor (RAF) approach for pooled human liver microsomes (HLM). This study could contribute to the understanding of the pharmacological activity and hepatotoxicity of DB.

DMD Fast Forward. Published on July 22, 2014 as DOI: 10.1124/dmd.114.058222
This article has not been copyedited and formatted. The final version may differ from this version.

Materials and Methods

Chemicals and Reagents

DB (> 98% purity) was purchased from Shanghai Forever Biological Technology Co., LTD. (Shanghai, China). Glucose 6-phosphate, glucose-6-phosphate dehydrogenase, NADPH, Tris base, reduced GSH, methoxylamine, sulfaphenazole, and (S)-(+)-N-3-benzylnirvanol were from Sigma-Aldrich (St. Louis, MO, USA). Human enzymes CYP1A2, 2A6, 2B6, 2C8, 2C9, 2C18, 2C19, 2D6, 2E1, 3A4, 3A5, and human CYP-reductase coexpressed in *Escherichia coli*, supplemented with purified cytochrome B5, were from Shanghai Ruide Institute of Liver Disease (Shanghai, China). Pooled HLM of 32 humans (with equal numbers of males and females) were from BD Biosciences (Woburn, MA, USA). Ketoconazole and jatrorrhizine hydrochloride (Internal standard, IS) were purchased from the National Institute for Food and Drug Control (Beijing, China). Ultrapure water (> 18 mΩ) was obtained from a Milli-Q water purification system (Millipore, MA, USA). HPLC-grade acetonitrile was purchased from Fisher Scientific (Fair Lawn, NJ, USA). NMR solvents used were 99.8% ampoule DMSO-*d*6 or pyridine-*d*5 (Cambridge Isotope Laboratories Inc., MA, USA). All other chemicals used were of analytical grade.

Animals. Male Sprague-Dawley rats (weighing 200 g to 250 g) were purchased from Shanghai Slac Laboratory Animal Co. Ltd (Shanghai, China). All experiments performed in rats were in accordance with the P.R. China legislation on the use and care of laboratory animals and approved by Experimental Animal Ethical Committee, Shanghai University of Traditional Chinese Medicine.

Preparation of Liver Microsomes

Liver microsomes were prepared from Sprague-Dawley rats, mice, rabbits, and guinea pigs according to the reported method (Lu et al., 1972). The method used un-induced animals, as well as animals that were pretreated with phenobarbital (50 mg/kg, intraperitoneally, for 3 d). Protein concentrations were determined according to the method described by Bradford (1976).

Microsomal Incubations

Incubation system (100 μL) contained DB (100 μM), microsomal proteins (1 mg/mL), and NADPH-regenerating system that included NADPH (1 mM), glucose 6-phosphate (10 mM), and glucose-6-phosphate dehydrogenase (1 unit/mL), in buffer A (50 mM Tris-HCl, pH 7.4, containing 4 mM $MgCl_2$) or buffer B (100 mM phosphate buffer, pH 7.4, containing 4 mM $MgCl_2$). DB was dissolved in acetonitrile, and the final concentration of acetonitrile in the incubation system was < 1%. The system was pre-incubated for 5 min at 37°C and initiated by adding NADPH. Control incubations were conducted without DB or NADPH. Incubations were stopped after 1 h by the addition of 500 μL ice-cold acetonitrile and then vortex-mixed for 1 min. Denatured proteins were separated by centrifugation at 16000 × *g* for 10 min. The supernatant (540 μL) was evaporated to dryness under a nitrogen stream, reconstituted using 90 μL of 10% acetonitrile, vortex-mixed for 1 min, and centrifuged at 16000 × *g* at 4°C for 10 min. The supernatant (5 μL) was injected into the UPLC-MS system for analysis (*see analysis A*).

Trapping experiments were conducted in the presence of nucleophiles, including GSH and methoxylamine (each at 10 mM), and the samples were prepared by the above-stated procedure.

Metabolism *in vivo* in Rats

Investigation of Metabolites in Plasma of Rats. Male rats were fasted for 12 h and had free access to water prior to the experiments. Blank blood samples were drawn from the retro-orbital plexus before administration. Then, DB formulated in 0.5% methylcellulose suspension was orally administrated by gavage to rats in single doses of 32, 75, and 150 mg/kg. Blood samples (~300 μL) were drawn at 0.5, 1.0, 2.0, 4.0, 8.0, 12.0, and 24 h after DB administration. Plasma was generated by centrifugation at 10000 × *g* for 5 min. Acetonitrile (5 mL) was added to the combined plasma (1 mL) to precipitate the protein, then vortex-mixed for 1 min, and centrifuged at 16000 × *g* for 10 min. The supernatant was evaporated to dryness under nitrogen stream, reconstituted using 200

μL of 10% acetonitrile, vortex-mixed for 1 min, and centrifuged at 16000 × *g* at 4°C for 10 min. The supernatant (5 μL) was injected into the UPLC-MS system for analysis (*see analysis A*).

Investigation of Metabolites in Urine and Feces of Rats. Rats were treated as described above. Blank urine, feces before dosing, and urine and feces from 0 h to 24 h after dosing were collected and stored at -80°C until analysis. Urine (1 mL) was processed using the procedure used to process the plasma. Feces were moistened with little water and then homogenized. All homogenated feces were extracted using 6-fold acetonitrile by ultrasonic wave for 1 h and then centrifuged (Yang et al., 2013). The supernatant (100 μL) was diluted with 100 μL water, and a 5 μL aliquot of the diluted solution was injected into the UPLC-MS system for analysis (*see analysis A*).

Investigation of Biliary Metabolites in Rats. Rats were terminally anesthetized with urethane (1.4 g/mL in isotonic saline; 1.0 mL/kg intraperitoneally) and cannulated via the bile duct. DB was suspended in 0.5% methylcellulose and injected into the stomach in a single dose of 75 mg/kg. Drug-free bile was collected for 30 min before DB administration. Bile was then collected from 0 h to 4 h and 4 h to 8 h after administration. Bile samples were prepared similar to the plasma and urine samples as described above.

UPLC-MS Analysis to Screen Metabolites *in vitro* and *in vivo* (*analysis A*). Samples from incubation and biological specimens (plasma, bile, urine, and feces) were analyzed on an Agilent 6410 Triple Quad LC-MS/MS system (Agilent Technologies Inc., USA) or Waters ACQUITY UPLC-Micromass Q-TOF system (Waters, Manchester, UK) using an Acquity UPLC^{TM} BEH C_{18} column (50 × 2.1 mm, 1.7 μm) (Waters, Milford, MA, USA) at 40°C. The analytes were separated by a gradient mobile phase consisting of acetonitrile (A) and aqueous solution of 0.1% formic acid (B) at the flow rate of 0.2 mL/min. The gradient elution program was as follows: 0 min to 15.0 min, 5% to 25% A; 15.0 min to 16.0 min, 15% to 80% A; 16.0 min to 17.0 min, 80% to 5% A (program A) or 0 min to 5.0 min, 10% to 20% A; 5.0 min to 12.0 min, 20% to 27% A; 12.0 min to15.0

min, 27% to 95% 15.0 min to 17.0 min, 95% to 5% A (program B). The temperature of the autosampler was maintained at 3°C to 6°C. MS was operated in positive mode under the following operating Triple Quad parameters: gas temperature, 325°C; gas flow, 10 L/min; nebulizer, 35 psi; capillary voltage, 4.0 kV; fragmentor, 130 V; cell accelerator, 3 V; dwell, 200 ms. For Q-TOF, the parameters were as follows: capillary voltage, 3.0 kV; sampling cones, 20 V; extraction cone, 4.0 V; source temperature, 120°C; desolvation temperature, 350°C; cone gas 50 h/Lr; and desolvation gas 600 h/Lr.

Elemental composition calculations for the exact masses were performed off-line using MassLynx V4.1, which was used to apply the spectrum that was manually generated for every peak. Potential assignments were calculated using monoisotopic masses with a tolerance of 10 ppm deviation. The number and types of expected atoms were set as follows: carbons ≤ 60, hydrogens ≤ 120, oxygens ≤ 30, nitrogens ≤ 30, and sulfurs ≤ 5.

Chemical Synthesis of Main Metabolites (GSH conjugates of DB)

Dimethyldioxirane (DMDO). DMDO was prepared according to the reported method (Murray and Singh, 1997) with slightly modified generator apparatus in which another Dewar condenser was connected to the receiving flask instead of the air condenser. Briefly, peroxymonosulphate (oxone, 50 g, 0.0813 mol) was added in portions to a stirred mixture of water (20 mL), acetone (12 mL, 0.163 mol), and sodium bicarbonate (24 g) under nitrogen atmosphere. An acetone (14 mL) - water (20 mL) mixture was simultaneously added dropwise. The reaction proceeded for 15 min, and a slight vacuum was applied to the reaction assembly. The distillate was collected for 20 min in the receiving flask containing Na_2SO4 and cooled in a dry ice/acetone bath. The receiving flask was also connected to a trap with potassium iodide solution. The distillate solution (3 mL to 4 mL), which typically afford DMDO concentrations of 0.02 M to 0.04 M, was transferred to a dry ice bath and used immediately for the next step.

Enedial Derivative of DB. DB (10 mg, 0.029 mmol) was dissolved in 2 mL acetone and pre-cooled in dry ice

bath for 1 min. Then, 1.2 mL DMDO was added immediately. The reaction mixture was allowed to warm up to room temperature and left to stand for 2 h. A 200 μL aliquot of the reaction mixture was evaporated to dryness under nitrogen stream and reconstituted using 200 μL 10% acetonitrile for UPLC-MS analysis (*see analysis A*) to confirm the disappearance of DB. The residual DMDO was bubbled off in the stream of nitrogen gas. The total volume was reduced to 0.5 mL and used immediately for the next step.

Reaction of Enedial Derivative of DB with GSH. GSH (17.8 mg, 0.058 mmol) was dissolved in 2 mL phosphate buffer (pH 7.4), and a solution of enedial derivative of DB **(**0.5 mL) was added dropwise while shaking. The resulting solution was left to stand at room temperature for 15 min. A 10 μL aliquot of the solution was diluted with 1 mL water and then subjected to the UPLC-MS system (*see analysis A*) to confirm the production of GSH adducts of DB. The final solution was stored at -80°C until the following separation.

Semi-preparative HPLC Separation of Synthetic Products. The synthetic products were separated by RP-HPLC system using a DIKMA Spursil C18 column (250 × 10 mm, 5 μm) at 25℃, with mobile phase consisting of 25% acetonitrile and 0.1% formic acid at the following gradient flow rates: from 0 min to 15 min, 1.8 mL/min; and from 15 min to 35 min, 1.6 mL/min. The wavelengths were set at 210 and 254 nm.

Incubations of DB with Recombinant Human CYP450 Enzymes

Recombinant human liver CYP450 isoenzymes of 100 pmol/mL (CYP1A2, 2A6, 2B6, 2C8, 2C9, 2C18, 2C19, 2D6, 2E1, 3A4, and 3A5) were incubated with 50 μM DB in phosphate buffer solutions. The concentrations of GSH and NADPH-regenerating system were similar to those in microsomal incubations. The incubations (100 μL), which were conducted in triplicates, were stopped by the addition of 500 μL cold acetonitrile containing jatrorrhizine hydrochloride (IS) and following the steps of the microsomal incubations. Microsomes from the same cell line that contain only the vector were used as control. The formation rate of metabolite M31, one of the main MGCDs, was determined by UPLC-MS (*see analysis B*).

DMD Fast Forward. Published on July 22, 2014 as DOI: 10.1124/dmd.114.058222
This article has not been copyedited and formatted. The final version may differ from this version.

Incubations of DB with Pooled HLM and Specific Chemical Inhibitors

To estimate the importance of CYP450 enzymes responsible for the bioactivation of DB, DB (60 μM) was incubated with pooled HLM (0.2 mg/mL) in the presence of NADPH-regenerating system, GSH (10 mM), and chemical inhibitors at 37°C for 1 h. The chemical inhibitors used were as follows: sulfaphenazole (10 μM) for CYP2C9, (S)-(+)-N-3-benzylnirvanol (1 μM) for CYP2C19 (Walsky and Obach, 2003), and ketoconazole (1 μM) for CYP3A4/5 (Venkatakrishnan et al., 2001). Control incubations were conducted with vehicles but without chemical inhibitors. (S)-(+)-N-3-Benzylnirvanol was dissolved in DMSO, sulfaphenazole in water, and ketoconazole in methanol. Organic solvents in the incubations were controlled within 1% of the incubation volume. Incubations in triplicates were processed as described in incubations with recombinant human CYP450 enzymes. Inhibition was calculated as the M31 formation rate in the inhibited ($v_{inhibited}$) samples (n = 3) relative to the control ($v_{control}$) samples (n = 3):

$$\text{inhibition} = (1 - v_{inhibited}/v_{control}) \times 100.$$

Enzyme Kinetics Studies on the Formation of MGCD (M31)

Incubations used to derive kinetic constants by the formation of M31 had the following DB and P450/HLM concentrations: DB, 5, 10, 20, 40, 60, 80, 100, 120, 160, 200, and 300 μM; CYP3A4, 10 pmol; CYP3A5, 15 pmol; CYP2C9, 25 pmol; CYP2C19, 15 pmol; and pooled HLM, 0.2 mg/mL. Incubation solutions (100 μL), which were conducted in triplicates, were transferred to ice bath for 5 min after 1 h at 37℃, and then followed by the sequential addition of 10 μL acetonitrile containing jatrorrhizine hydrochloride (IS), 10 μL DMSO, and 480 μL acetonitrile. The following processing steps were similar to those of the microsomal incubations except that the residual was reconstituted with 90 μL aqueous solution of 10% DMSO and 10% acetonitrile. The samples were analyzed by UPLC-MS (*see analysis B*). The enzyme kinetic investigations were performed within the range of linearity with respect to concentrations of CYP450 enzymes and DB, which were determined in

DMD Fast Forward. Published on July 22, 2014 as DOI: 10.1124/dmd.114.058222
This article has not been copyedited and formatted. The final version may differ from this version.

preliminary experiments. Parent compound conversions were within 5% at all DB concentrations. Apparent K_m and V_{max} were estimated by nonlinear regression using GraphPad Prism 5.0 (GraphPad Software Inc., SanDiego, CA). The data were fitted to the one-enzyme Michaelis-Menten equation [$V = V_{max} \times S/(K_m + S)$] or the Michaelis-Menten model with uncompetitive substrate inhibition [$V = V_{max} \times S/(K_m + S + S^2/K_s)$] (Venkatakrishnan et al., 2001). Eadie-Hofstee transformations were utilized when multiple enzymes were involved or Hill equation was more suitable.

Prediction of Relative Contributions for CYP450 Enzymes in HLM to MGCD (M31) Formation

The relative contribution of CYP450 isoforms in HLM to the formation of M31 was predicted using RAFs (Crespi and Miller, 1999) that was calculated as $f_i(\%) = RAF_i\ v_i(s)/\sum RAF_i\ v_i(s) \times 100$, where f_i is the relative contribution of a specific CYP450 isoform, RAF_i is the relative activity factor, and v_i is the reaction velocity of the CYP450 isoform at a specific DB concentration. v_i was calculated by Michaelis-Menten equation using the estimated V_{max} and K_m. RAF_i was calculated as rate for a probe substrate in HLM divided by rate for a probe substrate with cDNA expressed. The probe substrates were testosterone, tolbutamide and (S)-mephenytoin for CYP3A4/5, CYP2C9, and CYP2C19, respectively.

UPLC-MS Analysis for MGCD (M31) Formation (*Analysis B*)

Chemically synthesized M31 was used as standard substance. The UPLC - MS/MS method was fully validated according to the Bioanalytical Method Validation Guide enacted by the Food and Drug Administration (U.S. Department of Health and Human Services, 2001). Analysis was performed on an Agilent 6410 Triple Quad LC-MS/MS system (Agilent Technologies Inc., USA) using an Acquity UPLC™ BEH C_{18} column (50 × 2.1 mm, 1.7 μM; Waters, Milford, MA, USA) at 40°C. The analytes were separated by a gradient mobile phase consisting of acetonitrile (A) and aqueous solution of 0.1% formic acid and 5 mM ammonium acetate (B) at the flow rate of 0.3 mL/min. The gradient elution program was as follows: 0 min to 4.0 min, 10% to 16.4% A; 4.0

min to 6.0 min, 16.4% to 40% A; 6.0 min to 8.0 min, 40% to 80% A; and 8.0 min to 10.0 min, 80% to 10% A. The temperature of the auto-sampler was maintained at 4°C. The injection volume was 5 μL. MS/MS system was operated in positive mode under the following operating parameters: gas temperature, 325°C; gas flow, 10 L/min; nebulizer, 35 psi; capillary voltage, 4.0 kV; fragmentor, 190 V for M31 and 170 V for IS; cell accelerator, 3 V for M31 and 1V for IS; and dwell, 200 ms. Quantification transitions for multiple reaction mode (MRM) were set at *m/z* 632.1→*m/z* 557.2 for M31 and *m/z* 230.1→*m/z* 120.9 for IS, with collision energy set to 20 V for both substances. The data were processed using the Agilent MassHunter Qualitative Analysis B.04.00 Software (Agilent Technologies Inc., USA). Calibration standards with seven levels (0.083, 0.166, 0.332, 0.83, 1.66, 3.32, and 6.64 μM) were prepared daily by adding stock solution of M31 (86 μM) by serial dilutions. Calibration standards were analyzed in triplicates, and quality control samples at three levels (0.083, 0.332, and 3.32 μM) were run daily and checked to confirm that they were at nominal value.

Results

Identification of Metabolites in Microsomal Incubations

Thirteen (13) metabolites dependent on the NADPH-regenerating system were detected in the microsomal incubations (Fig. 1). These metabolites included 11 metabolites in buffer A and two in buffer B.

M1 to M3. Metabolites M1 to M3 were observed at *m/z* 464.2 ($M + H^+$), with a chemical formula of $C_{23}H_{29}NO_9$ by Q-TOF mass, which indicated that one molecule of Tris base ($C_4H_{11}NO_3$) might be conjugated to DB. M1 to M3 were identified as Tris base conjugates of DB formed via reactive metabolites (Fig. 2) with a proposed mechanism (Fig. 3) similar to the bioactivation of teucrin A (Druckova and Marnett, 2006). The furan moiety of DB was catalyzed by CYP450 to form reactive metabolites, 2-butene-1,4-dial derivatives of DB, and one of the aldehyde groups of the reactive metabolites reacted with the amine group of Tris base to form the Schiff base. The Schiff base then reacted with the other aldehyde group of the reactive metabolite via addition

reaction, and intramolecular rearrangement occurred to form substituted pyrrol derivatives. Signals of fragments with loss of H_2O, CO, or C $(CH_2OH)_3$ were observed (Table 1, Fig. 4), supporting the deduced structures of M1 to M3. According to the synthesis of the conjugates of tecucrin A with *N*-acetyl lysine (Druckova and Marnett, 2006), the configuration of C12 in DB could be changed in the metabolites. The 3-substituted pyrroline-2-one could be the major metabolites (M3), similar to the main conjugates of tecucrin A with *N*-acetyl lysine. M1 to M3 might be composed of four compounds which having two structures, 3-substituted pyrroline-2-one and 4-substituted pyrroline-2-one, with different configurations in C12 (Fig. 2). But, it's difficult to distinguish each one from mass data except the major metabolites (M3).

M4 to M6. Metabolites M4 to M6 exhibited a signal at *m/z* 360.1 ($M + H^+$), 15 Da higher than DB in molecular weight. Signals of fragments *m/z* 332.0 ($M + H^+$-CO), *m/z* 314.2 ($M + H^+$-CO-H_2O), and *m/z* 286.0 ($M + H^+$-CO-H_2O-CO) were observed, which demonstrated similar DB fragmentation. From their chemical formula ($C_{19}H_{21}NO_6$), metabolites M4 to M6 were deduced as the *N*-dealkylated products of M1 to M3 with a loss of $C(CH_2OH)_3$ (Fig. 2).

M7 to M9. Metabolites M7 to M9 were observed at *m/z* 446.2 ($M + H^+$), 18 Da lower than that of M1 to M3, suggesting that intramolecular reaction might occur when Tris base conjugated to the reactive metabolites of DB (Fig. 2). This reaction is probably similar to the formation of M27 to M31 (see *"M27 to M31"*). However, no fragment signals were observed, which resulted in the deduction with slight uncertainty.

M10 and M11. Metabolites M10 and M11 showed signals at *m/z* 378.2 ($M + NH_4^+$), with similar parent ion of DB (*m/z* 362.2, $M + NH_4^+$) and similar DB fragmentation patterns (Table 1). Thus, M10 to M11 were identified as the mono-oxydates of DB.

M12 and M13. Microsomal incubations of DB in buffer B (phosphate buffer) generated two other products M12 and M13 (*m/z* 377.2, $M + H^+$), in addition to M10 and M11, with the disappearance of M1 to M9 when

DMD Fast Forward. Published on July 22, 2014 as DOI: 10.1124/dmd.114.058222
This article has not been copyedited and formatted. The final version may differ from this version.

buffer A (Tris buffer) was replaced. M12 and M13 were also involved in the formation of reactive metabolite and were identified as hemiacetal lactones (*see identification of the synthesized products*). The 2-butene-1,4-dial moiety of the reactive metabolite turned into hemiacetal and was oxidized to hemiacetal lactones (Fig. 2).

M1 to M13 were all observed in the incubations with liver microsomes of rabbits and guinea pigs, and M11 was absent in the microsomal incubations of rats, mice, and human.

Trapping experiments using methoxylamine in buffer A with rat liver microsomes (RLM) resulted in a series of metabolites (M14 to M26, Fig. 5) along with the disappearance of M1 to M9.

M14 to M16. Metabolites M14 to M16 were observed at *m/z* 360.2 ($M+H^+$), with similar chemical formulae ($C_{19}H_{21}NO_6$) and fragments (Table 1) with M4 to M6, as well as similar DB relative retention times. M14 to M16 were identified as *N*-dealkylated products of conjugates of methoxylamine and DB (Fig. 6), consistent with M4 to M6.

M17 to M20. Metabolites M17 to M18 and M19 to M20 had the same parent ion signals at *m/z* 390.2 ($M + H^+$), with different fragment signals. Fragments with loss of CH_3OH (32 Da) were found in the MS spectra of M19 and M20, but were absent in M17 and M18, indicating that they had different structures. M17 and M18 were assigned as 3-substituted or 4-substituted *N*-methoxy pyrroline-2-one, which was deduced from their fragmentation pattern similar to that of M14 to M16. According to the NMR analysis of similar metabolites L-739, 010 (Zhang et al., 1996), M19 and M20 were deduced as 1-*O*-methyloxime-2-butene 4-aldehyde derivative of DB (Fig. 6), and the double-bond between carbon and nitrogen in the structures could turn into triple bond after losing CH_3OH. Their reduction products, M21 and M22, also supported the deduced structures. M19 and M20 could transform into M17 and M18 by intramolecular reaction.

M21 and M22. Metabolites M21 and M22 had an *m/z* 2Da higher than M19 and M20 and were eluted earlier than M19 and M20, suggesting they were reduction products of M19 and M20. Thus, M21 and M22 were

DMD Fast Forward. Published on July 22, 2014 as DOI: 10.1124/dmd.114.058222
This article has not been copyedited and formatted. The final version may differ from this version.

deduced as 1-*O*-methyloxime-2-butene 4-alcohol derivatives of DB.

M23 to M26. Metabolites M23 to M26 were observed at *m/z* 419.2 ($M + H^+$), 29 Da higher than that of M19 and M20. Chemical composition ($C_{21}H_{26}N_2O_7$) of M23 to M26 indicated that two molecules of methoxylamine were conjugated to DB. Fragmentation with loss of one molecule of CH_3OH (32 Da) from *m/z* 419.2 to *m/z* 387.2 suggested that M23 to M26 might have structures similar to M19 and M20. M23 to M26 were identified as the bis-*O*-methyloxime derivatives of DB, supported by their fragmentation with loss of another molecule of CH_3OH (32 Da) from *m/z* 341.2 to *m/z* 309.1 (Table 1).

The same GSH adducts (M27 to M35, Fig. 7) in other trapping experiments using GSH as capture reagent in buffer A or buffer B with RLM.

M27 to M31. The major metabolites M27 to M31 exhibited an *m/z* 632.2 ($M + H^+$) with chemical composition of $C_{29}H_{33}N_3O_{11}S$, which indicated that one molecule of GSH conjugated to DB and supported by the fragment signal (*m/z* 557.2) with loss of glycine. They were generated by intramolecular reaction after GSH conjugated to the 2-butene-1, 4-dial derivatives of DB (Lu et al., 2009) (Fig. 8). The main metabolite, M31, was composed of 3-mercapto-pyrrol (M31a) and 2-mercapto-pyrrol derivatives of DB (M31b) (*see identification of the synthesized products*). Similar to M1 to M3, the configuration of C12 could be changed in GSH conjugates of DB. Configurations of chiral carbons in GSH moieties also could be changed (*see identification of the synthesized products "another MGCD"*). Therefore, M27 to M30 might be composed of isomers of M31a and M31b with configurations changed in C12 or in GSH moiety.

M32 to M34. The metabolites M32 to M34 with signals at *m/z* 650.2 ($M + H^+$) were generated by GSH conjugated to DB similar to the formation of M1 to M3 (Fig. 8). These metabolites are supported by their chemical formula ($C_{29}H_{35}N_3O_{12}S$) and the fragment signal (*m/z* 575.2) with loss of glycine.

M35. A minor metabolite M35 was observed at *m/z* 939.2 ($M + H^+$). Its chemical formula ($C_{39}H_{50}O_{17}N_6S_2$), as

well as fragment signals with loss of one glycine (*m/z* 864.2) and two glycines (*m/z* 789.2) from parent molecule, indicated that two molecules of GSH were conjugated to DB. According to the formation of bis-GSH adducts of furan that were chemically synthesized (Chen et al., 1997), M35 was identified as bis-GSH conjugate of DB. This metabolite was formed by the mercapto group of one GSH added to the Schiff base that formed by the other GSH added to the aldehyde group of the reactive metabolites (Fig. 8).

Identification of Metabolites of DB *in vivo* in Rats

No metabolite but DB was found in the plasma of rats after oral administration at three dosages, compared with the blank plasma. Signal of mono-oxydate (M10) in the urine of rats was observed when DB was administered at 32 and 75 mg/kg. Several metabolites (M36 to M38) with signals at *m/z* 377($M + H^+$), in addition to M12 and M13, were observed in the feces of rats when DB was administered at 32 mg/kg (Fig. 9). M36 to M38, which could not be identified by mass data, might be the isomers of M12 and M13. Mono-GSH adducts (*m/z* 632, $M + H^+$), including M27, M30, and M31 were detected in the bile and feces of rats at DB dosages of 75 and 150 mg/kg.

Identification of the Synthesized Products

The reaction mixture exposed to air or not would result in different products before the residual DMDO was bubbled off in the stream of nitrogen gas (*see Enedial derivative of DB*). **M12** and **M13** (*m/z* 377) were the main products if the reaction mixture was exposed to air for a few minutes before it was concentrated under nitrogen. Otherwise, GSH adducts (*m/z* 632 and 939) were primarily produced if the reaction mixture was kept from air as long as possible (Fig. 10). M27, M31 and M35 could be observed in the total ion current (TIC) spectrum, while minor M28 to M30 could only be observed in the extract ion spectrum.

M12 and **M13** (with proportion of 5:1) were eluted from the column at 21.3 and 24.6 min, respectively. **M12** and **M13** were then lyophilized to afford white powder and each was composed of two isomers. Most signals in

DMD Fast Forward. Published on July 22, 2014 as DOI: 10.1124/dmd.114.058222
This article has not been copyedited and formatted. The final version may differ from this version.

the ^{13}C-NMR spectrum of **M12** are similar to those of DB (Yonemitsu et al., 1993) except that the signals belong to the furan moiety of DB change to those of one carbonyl of ester (δ171.23 for **M12a**, δ171.38 for **M12b**), one hemiacetal group (δ 99.49 for **M12a**, δ 98.50 for **M12b**), and one alkene group (δ 169.99 and 117.31 for **M12a**; δ 169.38 and 118.29 for **M12b**). **M12a** and **M12b** were identified as hemiacetal lactones with the hemiacetal group connected to the quaternary carbon of the alkene group. In **M13a** and **M13b**, the hemiacetal group (δ 99.00 for **M13a** and M13**b)** was linked to the methyne carbon of the alkene group (δ 135.70 and 147.46 for **M13a**; δ 137.15 and 147.33 for **M13b**). The configurations of C16 in **M12a** and **M12b** were determined to be R and S using the Chem3D Ultra 8.0 software (CambridgeSoft Corporation, USA), according to the differences in the chemical shifts of H11. The configurations of C15 in **M13a** and **M13b** were elucidated to be R and S by the same method (Fig. 10). The chemical shifts of C and H of **M12** and **M13**, attributed by the ^{1}H-^{1}H COSY, HSQC, and HMBC spectra, are shown in Table 2.

M31 was eluted from the column at 28.6 min, and then lyophilized to afford white powder. Signals similar to those of DB in the ^{13}C-NMR spectrum were all doubled, which indicated that **M31** is composed of two isomers (see Fig. 10 and supplemental Figure 1). The proportions of **M31a** and **M31b** were estimated to be approximately 1.2:1 according to the peak area of similar ^{1}H-NMR signals. **M31a** is 3-mercapto substituted of the pyrrole moiety supporting by the HMBC correlation between H12 (δ 5.36, dd) and the quaternary carbon (δ 107.11) (see supplemental Figure 2). **M31b** is 2-mercapto substituted of the pyrrole moiety because no similar HMBC correlation was observed. Correlations between H12 and H20 (CH_3) in NOESY of **M31a** and **M31b** suggested that the configurations of C12 of **M31a** and **M31b** were consistent with that of DB (see supplemental Figure 3). NMR data of M31a and M31b are shown in Table 3.

Another MGCD, an analog of M31, was eluted at 30.3 min and then lyophilized to afford white powder. ^{1}H-NMR spectrum of this **MGCD** (data not shown) was very similar to that of **M31**. Correlations between H12

DMD Fast Forward. Published on July 22, 2014 as DOI: 10.1124/dmd.114.058222
This article has not been copyedited and formatted. The final version may differ from this version.

and H20 (CH_3) in NOESY spectrum were also observed, which suggests that the **MGCD** was composed of isomers of **M31a** and **M31b** with configurations changed in the GSH moiety. The ^{13}C-NMR spectrum of the **MGCD** was not acquired because of insufficient compound.

Incubations of DB with Recombinant Human CYP450 Enzymes

CYP3A4 and 3A5, as well as 2C19 and 2C9, were capable of bioactivating DB to **M31** with 3A4 having the highest catalytic activity (Fig. 11).

Incubations of DB with Pooled HLM and Specific Chemical Inhibitors

The inhibited reaction activities for the formation of **M31** caused by ketoconazole, sulfaphenazole, and (S)-(+)-*N*-3-benzylnirvanol were 87%, 15%, and 27%, respectively. The results indicated that CYP3A4 was the major enzyme responsible for the bioactivation of DB.

Enzyme Kinetics Studies on MGCD (M31) Formation

The best fit of data was obtained using Michaelis-Menten equation for enzyme kinetics with pooled HLM (Fig. 12). Eadie-Hofstee transformations showed no evidence of two-enzyme kinetics. CYP3A4, 3A5, 2C9, and 2C19 also exhibited Michaelis-Menten kinetics with no evidence of uncompetitive substrate inhibition. The enzyme kinetics parameters are shown in Table 4.

Prediction of Relative Contributions for CYP450 Enzymes in HLM to MGCD (M31) Formation

The RAF predictions were made at 5.0 and 40 μM DB. CYP3A5 was not included for the RAF calculations. Considering the low V_{max} and large K_m, as well as the low expression in HLM, the contribution of CYP3A5 was lower than that of CYP2C19. The relative contributions of CYP3A4 were approximately 83.3% and 81.3%. CYP2C9 contributed about 10.5% and 12.2%, higher than those of CYP2C19 (6.2% and 6.6%).

Discussion

DB metabolism *in vitro* and *in vivo* in rats, as well as the human enzymes involved, was first investigated. The

main metabolic pathway of DB was catalyzed by CYP3A4/5, 2C9, and 2C19 to generate the reactive metabolites, 2-butene-1,4-dial derivatives of DB, which were captured by nucleophiles such as Tris base, methoxylamine, and GSH or oxidized to hemiacetal lactones. Tris base conjugates of DB (M1 to M3) that were observed at the TIC spectrum of microsomal incubations in Tris-HCl buffer incubation system provided important information of the metabolism pathway of DB, compared with little data of metabolites in the phosphate buffer system. Tris base was used as buffer constituent and as trapping agent for the reactive metabolites of DB because Tris base could react with aldehyde to form the Schiff base (Cannon and Danison, 1978; Niedernhofer et al., 1997). The metabolites of DB found *in vivo* in rats were consistent with those observed in RLM incubations *in vitro*. M10 was found in rat urine and MGCD in rat bile and feces, as well as M12 and M13 in rat feces, which indicated that DB was also transformed into 2-butene-1,4-dial derivatives *in vivo*. DB metabolism in liver and intestine decreased the bioavailability of DB when the compound was orally administered. In addition, species metabolic difference was observed in the formation of mono-oxidates; the two mono-oxydates (M10 and M11) were found in rabbits and guinea pig and one (M10) in rats, mice, and human microsomal incubations. The results might have been caused by the varying expression of flavin-containing monooxygenases among these species (data not shown).

MGCD was finally synthesized because of the extremely low yield of metabolites in microsomal incubations. The concentration of DMDO was not measured in the procedure because DMDO rapidly escaped from the solution, and DMDO measurement is time-consuming (Murray and Singh, 1997). A 1.2-mL volume of DMDO solution was sufficient to oxidize 0.029 mmol of DB, suggesting that the concentration of DMDO was > 0.024 M. UPLC-MS was used, instead of ^{1}H-NMR as previously reported (Druckova and Marnett, 2006), to monitor the disappearance of DB that was oxidized by DMDO. Unexpectedly, several products with signals at *m/z* 377, including M12 and M13, were detected. Thus, M12 and M13 were successfully synthesized. The reaction was

completed in 15 min, and the major products (M31a and M31b) transferred to their isomers (M27 and M28) when the reaction continued, which made the separation more difficult. M27 and minor M28 to M30 were hard to be separated because they were always eluted out together. M35 (*m/z* 939), having poor stability because of mercapto group, was hard to be obtained as well.

The structures of the reactive metabolites of DB were confirmed by the structure elucidations of metabolites in the trapping experiments of Tris base, methoxylamine, and GSH. Although it was difficult to distinguish metabolites with different configurations, the structure elucidations from mass data and literatures made sense except that M7 to M9 were temporarily inferred due to their little mass data. Chemical synthesis of M12, M13, M35 and M27 to M31 proved the existence of reactive metabolites and finally the NMR data of M12, M13 and M31 confirmed the structures of reactive metabolites.

UPLC-MS with MRM was used to improve selectivity and sensitivity to determine MGCD in incubations. MGCD was insoluble in acetronitrile, but soluble in DMSO. DMSO (10%) was used to reconstitute the residual to determine MGCD in enzyme kinetic samples, which resulted in high recoveries (90% to 110%) of MGCD. Prior to protein precipitation, 10 μL DMSO was added to keep the same procedure with calibration samples.

CYP3A4 was identified as the major bioactivation enzyme of DB both by chemical inhibition studies and RAF approach. Considering that RAF approach provides a satisfactory prediction of the roles of CYP450 isoforms compared with inhibition studies, contribution of CYP2C9 to the bioactivation of DB was higher than that of CYP2C19. However, the result in RAF approach was contrary to those from the inhibition studies. The contrasting results may have been caused by the compensation effects from other enzymes when CYP2C9 was inhibited. The K_m of CYP3A4 in the formation of M31 was 68.1 μM, indicating that DB had moderate affinity to CYP3A4.

DB and teucrin A both are bioactivated in the furan moiety. Furan has already been proved to transform into

cis-2-butene-1,4-dial by CYP450 (Chen et al., 1995). This reactive substance, *cis*-2-butene-1,4-dial is likely responsible for the ultimate toxic and carcinogenic properties of furan because it readily reacts with amino acid (Chen et al., 1997) and DNA (Byrns et al., 2006). Mono-GSH adduct of furan, as well as metabolites derived from cysteine *cis*-2-butene-1,4-dial lysine cross-links, was found in rat urine, which suggested that furan was also bioactivated to form *cis*-2-butene-1,4-dial *in vivo* (Peterson et al., 2006; Lu & Peterson, 2010). A substantial amount of radioactive materials remained in the liver bound to proteins at 24 h after dosing 8 mg/kg [^{14}C] furan to rats, which could cause hepatotoxicity in rats (Burka et al., 1991). Hepatotoxicity is correlated with covalent binding to hepatic proteins with reactive metabolites, which also has been clarified from numerous drugs. Acetaminophen is very safe at therapeutic doses. However, acetaminophen overdose may produce fulminating hepatic necrosis that can be fatal. Covalent binding resulting from reactive metabolites is the most important factor (Hinson et al., 2004). Troglitazone, an oral antidiabetic agent, has been removed from the market because it has been associated with cases of severe hepatotoxicity and drug-induced liver failure. Reactive metabolites may play a causative role (Kassahun et al., 2001). The bioactivation of DB that has been inferred to form reactive metabolites by liver CYP450 might be primarily responsible for the hepatotoxicity of DB and *D. Bulbifera*.

Previous studies have demonstrated that extract from *D. Bulbifera*, in which DB is the main ingredient, could cause higher hepatotoxicity to male than female mice (Wang et al., 2010). Pharmacokinetic studies revealed that the oral absolute bioavailability of DB in female rats was nearly 7 times higher than that in males (Yang et al., 2013). Given that DB was mainly metabolized by CYP3A4 in human, higher expression of 3A including 3A1 and 3A2 in male than females mice and rats (Kato and Yamazoe, 1992) could enhance more metabolized DB, resulting in higher hepatotoxicity in male mice and lower oral bioavailability in male rats than in females. Drug interaction should be noted that *D. Bulbifera* may cause fatal toxicity when used with inducers of CYP3A4 such

as rifampicin and hyperforin that also induce CYP2C9 expression (Harmsen et al., 2009; Chen et al., 2004).

The relation of the reactive metabolites with the antitumor activity of DB remains unknown. CYP450 expression, particularly, 1A, 1B, 2C, 3A, and 2D subfamily members, have been identified in a wide range of human cancers (Patterson and Murray, 2002). Prodrug antitumor agents that depend on CYP450 activation may also be activated in tumor regions. For example, AQ4N, a CYP3A substrate, is activated to a cytotoxic metabolite specifically in hypoxic tumor regions (Patterson and Murray, 2002). The relationship between reactive metabolites of DB and anti-tumor activity would be investigated in future studies.

Authorships contribution

Participated in research design: B.H. Yang, K.X. Chen, Z.T. Wang, and C.H. Wang

Conducted experiments: B.H. Yang and W. Liu

Contributed new reagents or analytical tools: B.H. Yang, W. Liu and C.H. Wang

Performed data analysis: B.H. Yang, W. Liu, and C.H. Wang

Wrote or contributed to the writing of the manuscript: B.H. Yang, W. Liu, and C.H. Wang

References

Bradford MM (1976) A rapid and sensitive method for the determination of microgram quantities of protein utilizing the principle of protein-dye binding. *Anal Biochem* **72:** 248-254.

Byrns MC, Vu CC, Neidigh JW, Abad J, Jones RA and Peterson LA (2006) Detection of DNA adducts derived from the reactive metabolite of furan, cis-2-butene-1,4-dial. *Chem Res Toxicol* **19:** 414-420.

Burka LT, Washburn KD and Irwin RD (1991) Disposition of [^{14}C]furan in the male F344 rat. *J Toxicol Environ Health* **34**:245–257.

Cannon DJ and Danison PF (1978) A stabilised tris(hydroxymethyl)aminomethane adduct in reduced collagen. *Connect Tissue Res* **4:** 187-191.

Chen LJ, Hecht SS, and Peterson LA (1995) Identification of cis-2-Butene-1,4-dial as a microsomal metabolite of furan. *Chem Res Toxicol* **8:** 903-906.

Chen LJ, Hecht SS, and Peterson LA (1997) Characterization of amino acid and glutathione adducts of cis-2-Butene-1,4-dial, a reactive metabolite of furan. *Chem Res Toxicol* **10:** 866-874.

ChenY, Ferguson SS, Negishi M, and Goldstein JA (2004) Induction of human CYP2C9 by rifampicin, hyperforin, and phenobarbital is mediated by the pregnane X receptor. *J Pharmacol Exp Ther* **308:** 495-501.

Crespi CL and Miller VP (1999) The use of heterologously expressed drug metabolizing enzymes- state of the art and prospects for the future. *Pharmacol Ther* **84:** 121-131.

Druckova A and Marnett LJ (2006) Characterization of the amino acid adducts of the enedial derivative of teucrin A. *Chem Res Toxicol* **19:** 1330-1340.

Harmsen S, Meijerman I, Beijnen JH, and Schellens JHM (2009) Nuclear receptor mediated induction of cytochrome P450 3A4 by anticancer drugs: a key role for the pregnane X receptor. *Cancer Chemother Pharmacol* **64:** 35-43.

Hinson JA, Reid AB, McCullough SS, and James LP (2004) Acetaminophen-induced hepatotoxicity: role of metabolic activation, reactive oxygen/nitrogen species, and mitochondrial permeability transition. *Drug Metab Rev* **36:** 805-822.

Ida Y, Kubo S, Fujita M, Komori T, and Kawasaki T (1978) Furanoid-norditerpene aus Pflanzen der Familie Dioscoreaceae, V. Struktur der Diosbulbine D, E, F. G and H. *Liehigs Ann Chem* 818-833.

Kassahun K, Pearson PG, Tang W, McIntosh I, Leung K, Elmore C, Dean D, Wang R, Doss G, and Baillie TA (2001) Studies on the metabolism of troglitazone to reactive intermediates *in vitro* and *in vivo*. Evidence for novel biotransformation pathways involving quinone methide formation and thiazolidinedione ring scission. *Chem Res Toxicol* **14:** 62-70.

Kato R and Yamazoe Y (1992) Sex-specific cytochrome P450 as a cause of sex- and species-related differences in drug toxicity. *Toxicol Lett* **64/65:** 661-667.

Kawasaki T, Komori T, and Setoguchi S (1968) Furanoid- norditerpenes from Dioscorea plants, I. diosbulins A, B, and C from *Dioscorea bulbifera* L. *forma spontanea* Makino et Nemoto. *Chem Pharm Bull* **16:** 2430.

Komori T (1997) Glycosides from *Dioscorea Bulbifera*. *Toxicon* **35:** 1531-1536.

Liu H, Chou GX, Guo YL, Ji LL, Wang JM, and Wang ZT (2010) Norclerodane diterpenoids from rhizomes of Dioscorea bulbifera. *Phytochemisty* **71 :**1174 - 1180.

Lu AYH and Levin W (1972) Partial purification of cytochrome P-450 and P-448 from rat liver microsomes. *Biochem Biophys Res Commun* **46:** 1334-1339.

Lu D and Peterson LA (2010) Identification of furan metabolites derived from cysteine cis-2-Butene-1,4-dial lysine cross-links. *Chem Res Toxicol* **23:** 142-151.

Murray RW and Singh M (1997) Synthesis of expoxides using dimethyldioxirane: trans-stilbene oxide: [dioxirane, dimethyl - and oxirane, 2,3-diphenyl-, trans]. *Organic Syntheses* **74:** 91-100.

Niedernhofer LJ, Riley M, Schnetz-Boutaud N (1997) Temperature-dependent formation of a conjugate between tris(hydroxymethyl)aminomethane buffer and the malondialdehyde-DNA adduct pyrimidopurinone. *Chem Res Toxicol* **10:** 556 -561.

Niu ZM and Chen AY (1994) 16 cases report of toxic hepatitis caused by *Dioscorea bulbifera*. *Chin J Integr Tradit Western Liver Dis* **4:** 55-56.

Njuguna NM, Masimirembwa C, and Chibale K (2012) Identification and characterization of reactive metabolites in natural products-driven drug dDiscovery. *J Nat Prod* **75:** 507 - 513.

Patterson LH and Murray GI (2002) Tumour cytochrome P450 and drug activation. *Curr Pharm Des* **8:** 1335-1347.

Peterson LA, Cummings ME, Chan JY, Vu CC and Matter BA (2006) Identification of a cis-2-butene-1,4-dial-derived glutathione conjugate in the urine of furan-treated rats. *Chem Res Toxicol* **19:** 1138 -1141.

Venkatakrishnan K, Moltke LL, and Greenblatt DJ (2001) Human drug metabolism and the cytochromes P450: application and relevance of in vitro models. *J Clin Pharmacol* **41:** 1149-1179.

Wang G, Liu JS, Lin BB, Wang GK, and Liu JK (2009) Two new furanoid norditerpenes from *Dioscorea bulbifera*. *Chem Pharm Bull* **57:** 625-627.

Wang JM, Liang QN, Ji LL, Liu H, Wang, CH, and Wang ZT (2010) Gender-related difference in liver injury induced by *Dioscorea bulbifera* L. rhizome in mice. *Hum Exp Toxicol* **30:** 1333-1341.

Wang JM, Ji LL, White CJB, Wang ZY, Shen KK, and Wang ZT(2012) Antitumor activity of *Dioscorea-bulbifera* L. rhizome in vivo. *Fitoterapia* **83:** 388-394.

Walsky RL and Obach RS (2003) Verification of the selectivity of (+)*N*-3-benzylnirvanol as a CYP2C19 inhibitor. *Drug Metab Dispos* **31:** 343.

Yang BH, Wang XT, Liu W, Zhang Q, Chen KX, Ma YM, Wang CH, and Wang ZT (2013) Gender-related pharmacokinetics and absolute bioavailability of diosbulbin B in rats determined by ultra-performance liquid chromatography-tandem mass spectrometry. *J Ethnopharmacol* **149:** 810-815.

Yonemitsu M, Fukuda N, Kimura T, and Komori T (1993) Diosbulbin-B from the leaves and stems of *Dioscorea bulbifera*: ^{1}H - ^{1}H and ^{13}C - ^{1}H COSY NMR studies. *Planta Med* **59:** 577.

Zhang KE, Naue JA, Arison B, and Vyas KP (1996) Microsomal metabolism of the 5-lipoxygenase inhibitor L-739,010: evidence for furan bioactivation. *Chem Res Toxicol* **9:** 547-554.

Zhang YP, Gao W, and Gao HY (2008) Research progress of Dioscorea bulbifera Linn. *Mod Chinese Med* **10:** 34– 37.

Footnotes

This work was supported by the Doctoral Fund of Ministry of Education of China [20133107110012] awarded to Professor Chang-Hong Wang.

Figure legends

Fig. 1. The typical total ion current (TIC) (A) and extract ion spectra of *m/z* 464 (B), *m/z* 360 (C), *m/z* 446 (D), *m/z* 378 (E), and *m/z* 377 (F) from microsomal metabolites of diosbulbin B in Tris-HCl buffer (M1 to M11) and phosphate buffer (M12 and M13), using Agilent 6410 Triple Quad LC-MS/MS system with eluting program A

Fig. 2. Metabolic profile of diosbulbin B *in vitro* in Tris-HCl buffer (M1 to M11) and phosphate buffer (M12 and M13)

Fig. 3. Proposed mechanisms for the formation of Tris base conjugates with the enedial derivatives of DB (M1 to M3)

Fig. 4. Structural formula of M3, including its fragmentation as shown by its mass spectrum using Agilent 6410 Triple Quad LC-MS/MS system

Fig. 5. The typical TIC (A) and extract ion spectra of *m/z* 360 (B), *m/z* 390 (C), *m/z* 392 (D), and *m/z* 419 (E) from microsomal metabolites of diosbulbin B trapped by methoxylamine in Tris-HCl buffer, using Waters ACQUITY UPLC-Micromass Q-TOF system with eluting program A

Fig. 6. Metabolic profile of diosbulbin B *in vitro* trapped by methoxylamine in Tris-HCl buffer

Fig. 7. The typical TIC (A) and extract ion spectra of *m/z* 632 (B), *m/z* 650 (C), and *m/z* 939 (D) from microsomal metabolites of diosbulbin B trapped by GSH, using Waters ACQUITY UPLC-Micromass Q-TOF system with eluting program B

Fig. 8. Metabolic profile of diosbulbin B trapped by GSH

Fig. 9. Metabolites found in the feces of rats that were orally administered with DB at 32 mg/kg, using Agilent 6410 Triple Quad LC-MS/MS system with eluting program A (A) and 150 mg/kg using Waters ACQUITY UPLC-Micromass Q-TOF system with eluting program B (B).

Fig. 10 The typical TIC spectra of the chemically synthesized products M12 to M13 (A), MGCD, and M31 (B), using Agilent 6410 Triple Quad LC-MS/MS system with eluting program A and their structures

Fig. 11. Formation of metabolites M31 by recombinant human cytochrome P450 isoenzymes after incubation with 50 μM DB for 60 min. Data shown is the area obtained in the mass spectrum for M31 relative to the internal standard and normalized to the amount of P450 (average of triplicate determinations ± S.D.)

Fig. 12. Enzyme kinetics after incubation with 5 μM to 300 μM DB for 60 min. Data shows the mean of triplicate determination

Table 1 Mass spectral data for the metabolites and diosbulbin B

Compound	m/z	MS^2	HRMS (measured)	HRMS (calculated)	Chemical formular	Error(ppm)
Diosbulbin B	362.2 ($M+NH_4^+$)	317.2, 299.3, 271.4, 253.3	362.1618	362.1604	$C_{19}H_{20}O_6$	-3.9
M1-M3	464.2 ($M+H^+$)	446.3, 428.3, 418.0, 400.1, 372.3, 360.3, 332.1	464.1927-464.1939	464.1921	$C_{23}H_{29}NO_9$	-3.9[a]
M4-M6	360.1 ($M+H^+$)	332.0, 314.2, 286.0,	360.1438-360.1440	360.1447	$C_{19}H_{21}NO_6$	1.9[a]
M7-M9	446.2 ($M+H^+$)		446.1790-446.1797	446.1815	$C_{23}H_{27}NO_8$	5.6[a]
M10-M11	378.2 ($M+NH_4^+$)	333.3, 315.1, 287.2	378.1553, 378.1537	378.1553	$C_{19}H_{20}O_7$	4.2[a]
M12-M13	377.2 ($M+H^+$)	359.1, 331.1, 303.1, 274.9, 257.1, 228.9	377.1232, 377.1239	377.1236	$C_{19}H_{20}O_8$	1.1[a]
M14-M16	360.2 ($M+H^+$)	332.2, 314.2	360.1425-360.1525	360.1447	$C_{19}H_{21}NO_6$	6.1[a]
M17-M18	390.2 ($M+H^+$)	362.2, 344.2	390.1562, 390.1534	390.1553	$C_{20}H_{23}NO_7$	-2.3[a]
M19-M20	390.2 ($M+H^+$)	362.2, 330.2, 312.1	390.1561, 390.1544	390.1553	$C_{20}H_{23}NO_7$	2.3[a]
M21-M22	392.2 ($M+H^+$)	374.2, 343.2	392.1718, 392.1737	392.1709	$C_{20}H_{25}NO_7$	-7.1[a]
M23-M26	419.2 ($M+H^+$)	388.2, 387.2, 359.2, 349.1, 341.2, 309.1	419.1820-419.1838	419.1818	$C_{21}H_{26}N_2O_7$	-4.8[a]
M27-M31	632.2 ($M+H^+$)	557.2, 335.6 ($M+K^++H^+$)	632.1899-632.1933	632.1914	$C_{29}H_{33}N_3O_{11}S$	-3.5[a]
M32-M34	650.2 ($M+H^+$)	632.2, 575.2	650.1993-650.2010	650.2020	$C_{29}H_{35}N_3O_{12}S$	1.5[a]
M35	939.3 ($M+H^+$)	864.2, 789.2, 761.2, 470.1 ($M+2H^+$)	939.2762	939.2752	$C_{39}H_{50}O_{17}N_6S_2$	-1.1

[a] The absolute value of the error is the biggest.

Table 2 ^{1}H (600MHz) and ^{13}C-NMR(150MHz) data for M12a, M12b and M13a, M13b (Pyridine-*d*5)

C/H Number	M12a/M12b			M13a/M13b		
	δ_H	$J_{-H,H}$ values	δ_C	δ_H	$J_{-H,H}$ values	δ_C
C-1/H-1	1.50(m)		29.52/29.92	1.23(m)/1.43(m)		29.68/29.22
	1.84(m)			1.71(m)/1.82(m)		
C-2/H-2	4.76(dd)	5.5, 5.5	76.94	4.74(dd)	5.5, 5.5	76.74
C-3/H-3	1.72(d)	11.7	39.20	1.67(d)	11.5	39.00
	2.34(dd)	5.4, 11.7		2.33(dd)	5.5, 11.5	
C-4/H-4	2.79(d)	4.4	42.42	2.77(d)	5	42.19
C-5/H-5	1.99(d)	12.0	42.33	1.92(d)	11.7	42.07/41.98
C-6/H-6	4.78(d)	5.7	78.11/77.9	4.73(d)	6.0	77.66/77.60
C-7/H-7	2.13(d)	11.6	37.19	2.07(d)	11.6	37.12
	2.53(dd)	5.8, 11.6		2.51(dd)/2.49(dd)	5.5, 11.6	
C-8			90.02/90.22			90.05/89.96
C-9			45.73			45.55/45.47
C-10/H-10	2.50(m)		40.98	2.04(m)/1.92(m)		38.89
C-11/H-11	2.0(dd)/1.82(dd)	11.7, 12.1/11.4, 11.7	40.52/39.63	1.22(dd)/1.65(dd)	10.5, 11.5	40.75/40.38
	2.24(dd)/2.08(dd)	6.0, 12.1/5.3, 11.7		1.98(dd)/2.23(dd)	5.5, 11.5	
C-12/H-12	5.39(dd)/5.20(dd)	5.5, 10.5	76.55/76.83	5.20(dd)	5.5, 10.5	75.46/75.16
C-13			169.99/169.38			135.7/137.15
C-14	6.56(s)/6.79(s)		117.31/118.29	7.90(s)		147.46/147.33
C-15/H-15			171.38/171.23	6.52(s)/6.62(s)		99.00
C-16/H-16	6.46(s)/6.71(s)		99.49/98.5			170.82
C-17			177.08/176.75			176.77
C-18			176.03			175.88
C-20/3H	1.09(s)/1.06(s)		16.21/15.94	0.98(s)/0.99(s)		15.87/15.75

DMD Fast Forward. Published on July 22, 2014 as DOI: 10.1124/dmd.114.058222
This article has not been copyedited and formatted. The final version may differ from this version.

Table 3 ^{1}H (600MHz) and ^{13}C-NMR (150MHz) data for M31a and M31b (DMSO-*d*6)

C/H Number	M31a/M31b		
	δ_H	$J_{H,H}$ values	δ_C
C-1/H-1	1.67(m)		29.23/29.33
	1.93(m)		
C-2/H-2	4.82(dd)	5.2, 5.2	77.34
C-3/H-3	1.93(d)	11.3	38.76
	2.4(dd)	5.4, 11.3	
C-4/H-4	2.71(d)	4.6	41.98/41.90
C-5/H-5	2.19(d)	10.1	41.53/41.36
C-6/H-6	4.73(d)/4.75(d)	5.2	77.78/78.51
C-7/H-7	2.11(d)/2.21(d)	10.7	37.51/37.33
	2.32(dd)/2.43(dd)	5.4, 10.7	
C-8			89.53/90.08
C-9			45.77/45.71
C-10/H-10	1.67(m)	11.3, 11.7	39.23/39.10
C-11/H-11	1.94(dd)	5.4, 11.7	41.24
	2.00(dd)	5.2, 10.4	
C-12/H-12	5.36(dd)/5.28(dd)	5.2, 10.1	75.68/74.90
C-13			126.39/125.15
C-14/H-14	6.99(bs) for 3b		107.11/128.64
C-15/H-15	6.64(bs) for 3a		121.82/107.73
C-16/H-16	6.96(bs) /6.83(bs)		134.01/122.38
C-17			177.89
C-18			176.84
C-20/3H	1.22(s)		16.86/16.73
Glu (-COOH)			179.22
Glu α-CH	4.81(m)		61.75
Glu β-CH2	2.1-2.3(m)		29.33
Glu γ-CH2	2.1-2.3(m)		29.92
Glu (-CO-NH-)			
Cys α-CH	4.23(m)/4.01(m)		58.16/56.45
Cys β-CH2	2.97(m)/3.21(m)		35.9/33.57
	2.58(m)/2.81(m)		
Cys (-CO-NH-)			171.26/171.40
Gly CH2	3.62 (overlapped)		41.77
Gly (-COOH)			171.26/171.40

DMD Fast Forward. Published on July 22, 2014 as DOI: 10.1124/dmd.114.058222
This article has not been copyedited and formatted. The final version may differ from this version.

Table 4 Enzyme kinetic parameters for Diosbulbin B to M31

	V_{max}	K_m	V_{max}/K_m
HLM and CYPs	pmol·min^{-1}·mg^{-1} protein or pmol·min^{-1}·pmol^{-1} CYP	μM	L·min^{-1}·mg^{-1} protein or L·min^{-1}·pmol^{-1} CYP
HLM	776.2	254.0	3.06×10^{-3}
3A4	6.3	68.3	9.22×10^{-5}
3A5	2.0	98.5	2.03×10^{-5}
2C9	1.9	133.8	1.42×10^{-5}
2C19	6.3	92.0	6.85×10^{-5}

FIG 1

DMD Fast Forward. Published on July 22, 2014 as DOI: 10.1124/dmd.114.058222
This article has not been copyedited and formatted. The final version may differ from this version.

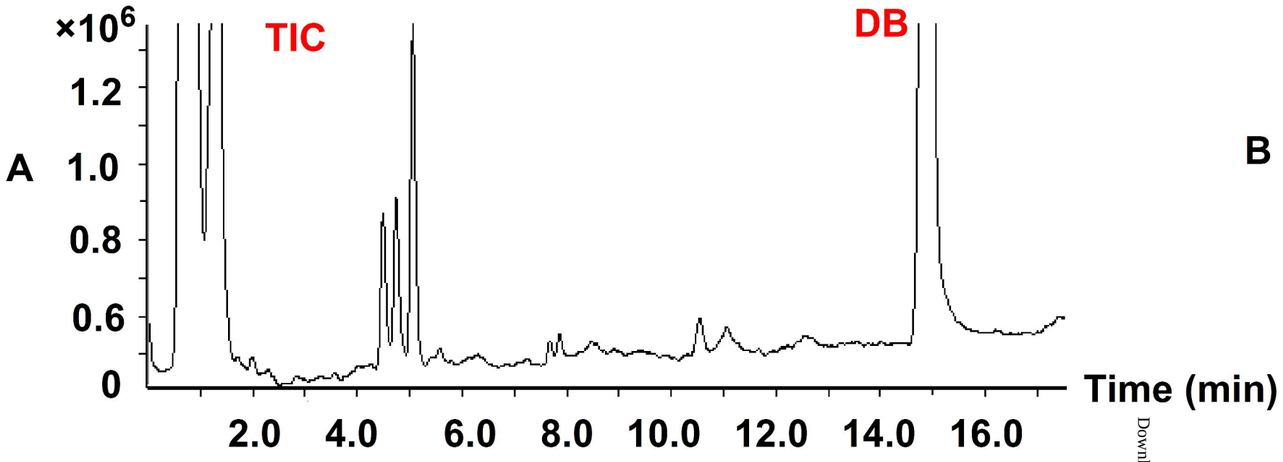

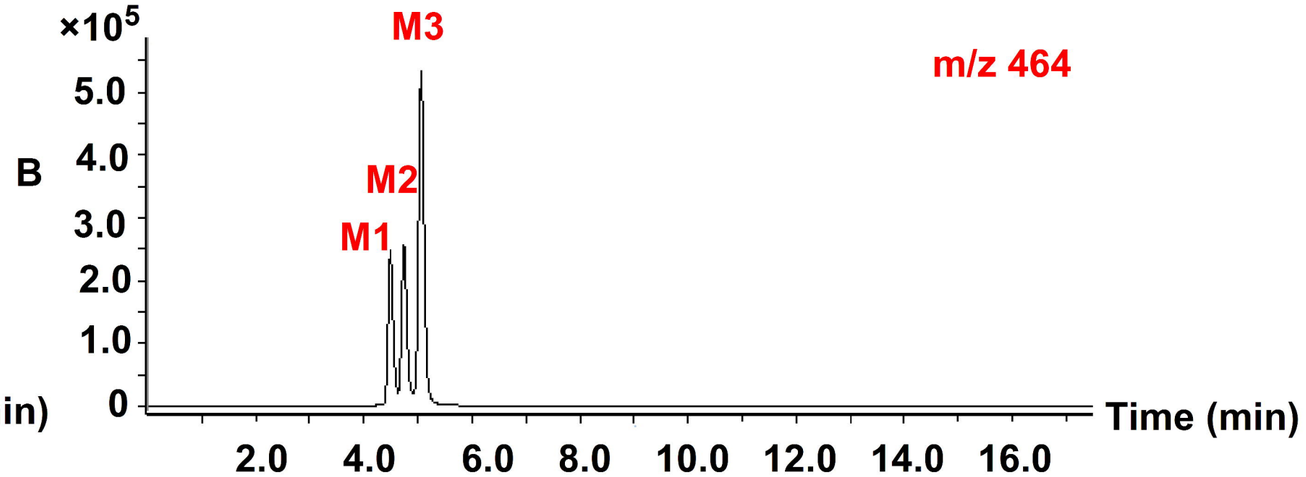

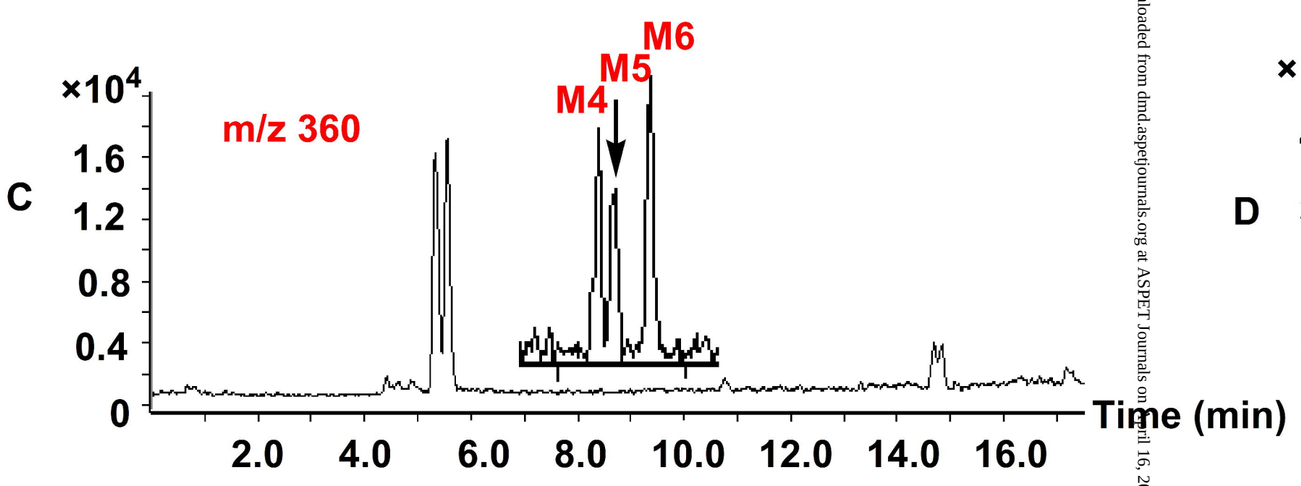

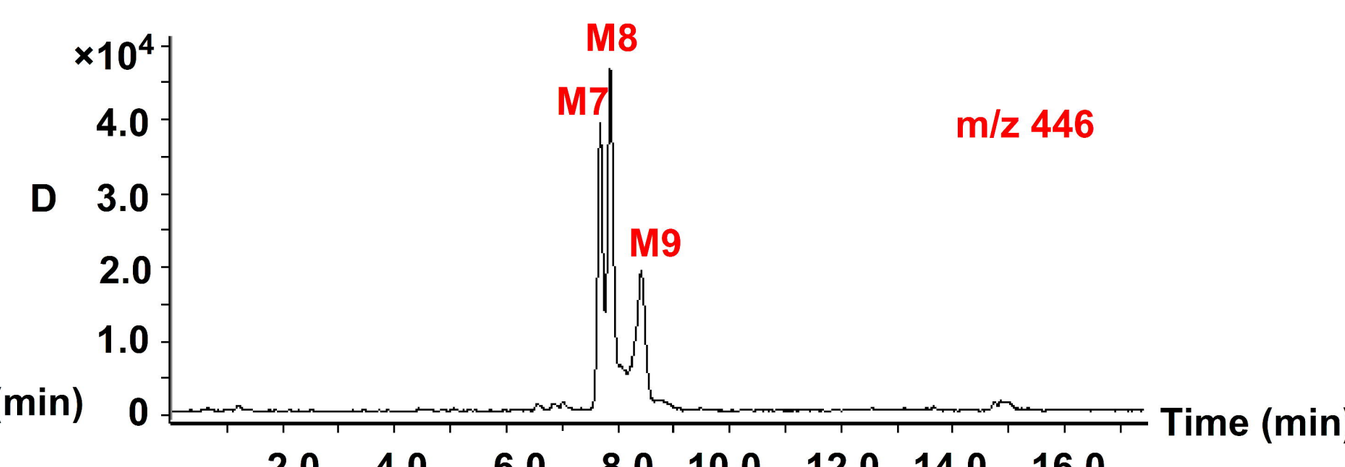

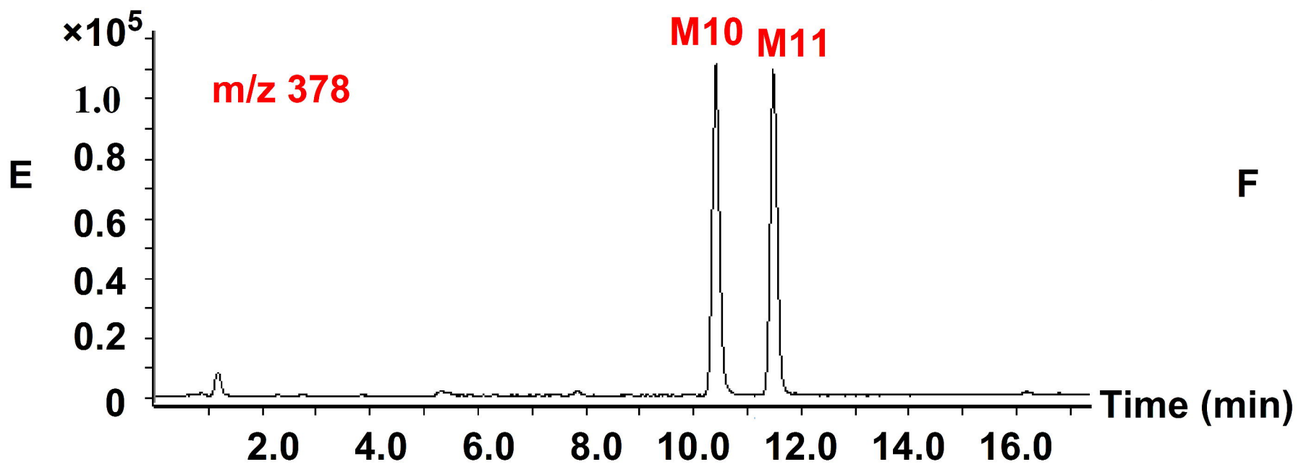

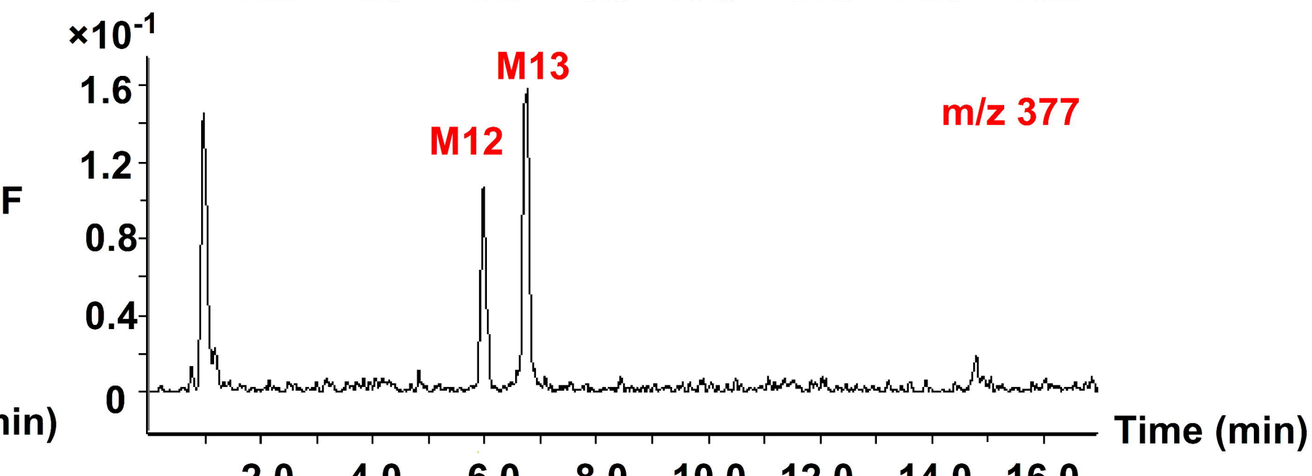

FIG 2

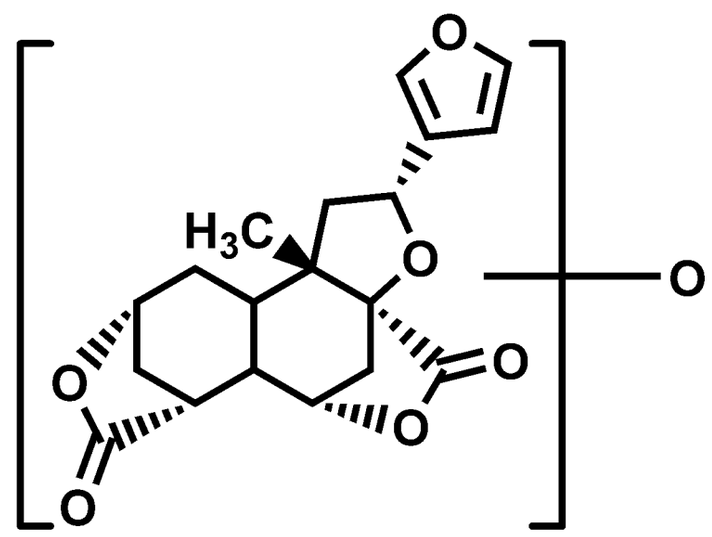

M10-M11

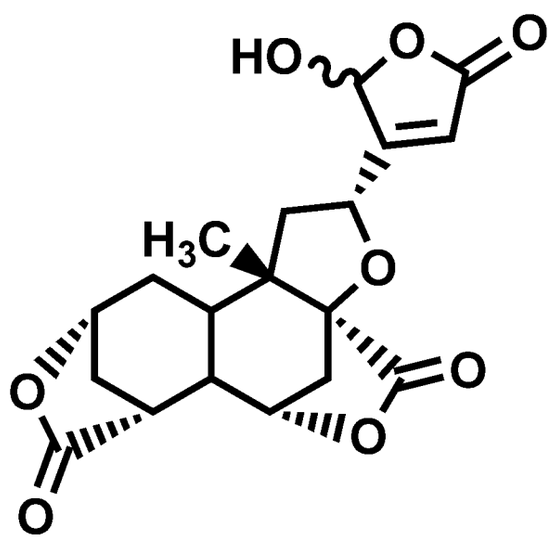

M12

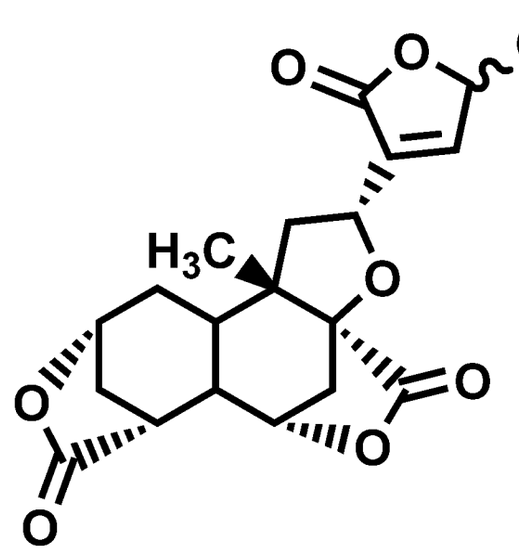

M13

[O]

[O]

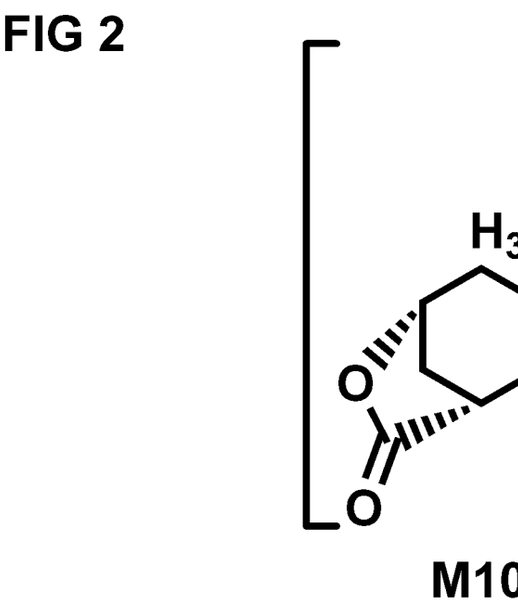

CYP3A4/A5

2C9/2C19

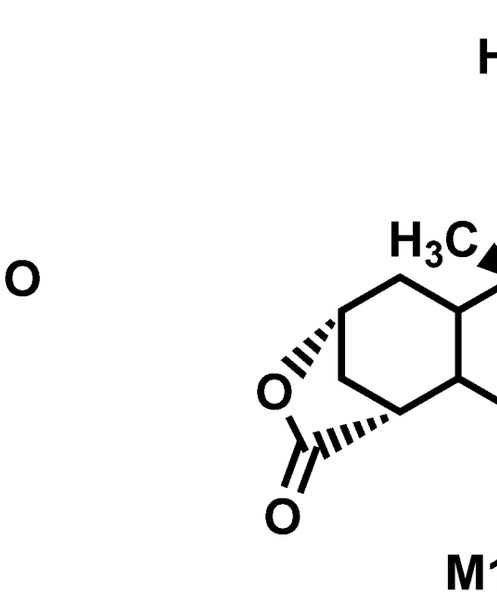

H_2O

Diosbulbin B (DB)

Tris base

DMD Fast Forward. Published on July 22, 2014 as DOI: 10.1124/dmd.114.058222

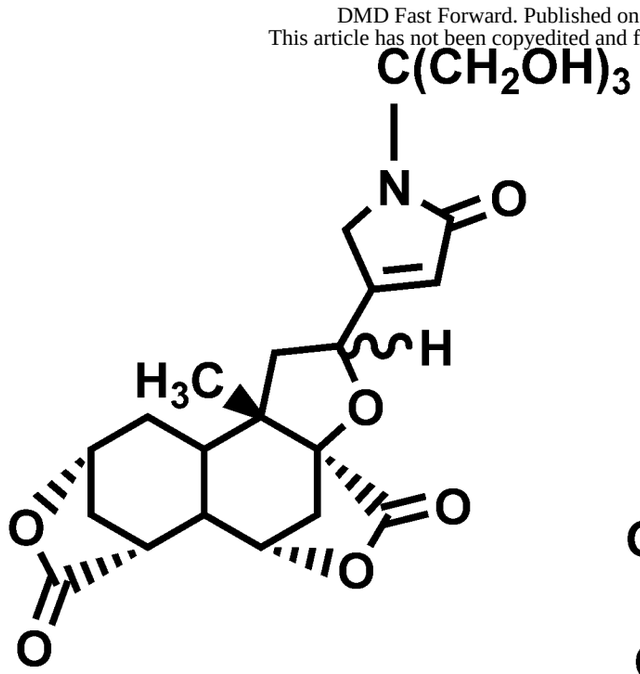

Minor

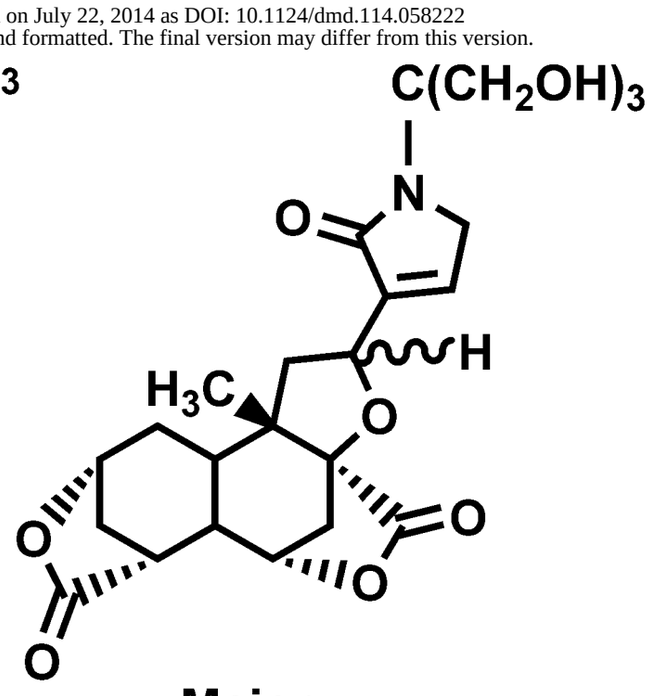

Major

M1-M3

+

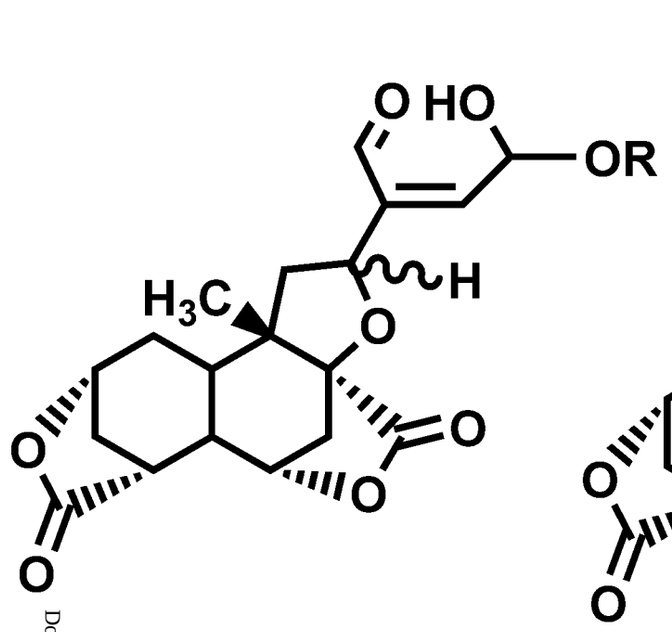

R=$CH_2C(CH_2OH)_2NH_2$

N-dealkylation

Intramolecular reaction

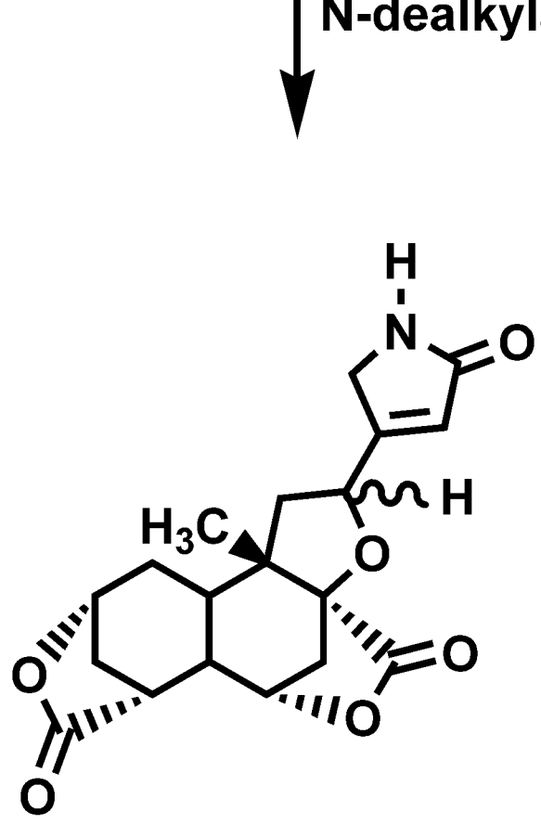

Mionr

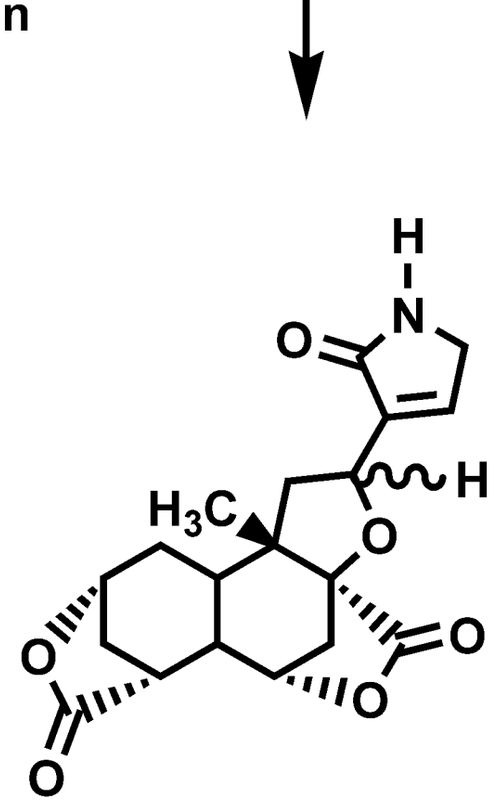

Major

M4-M6

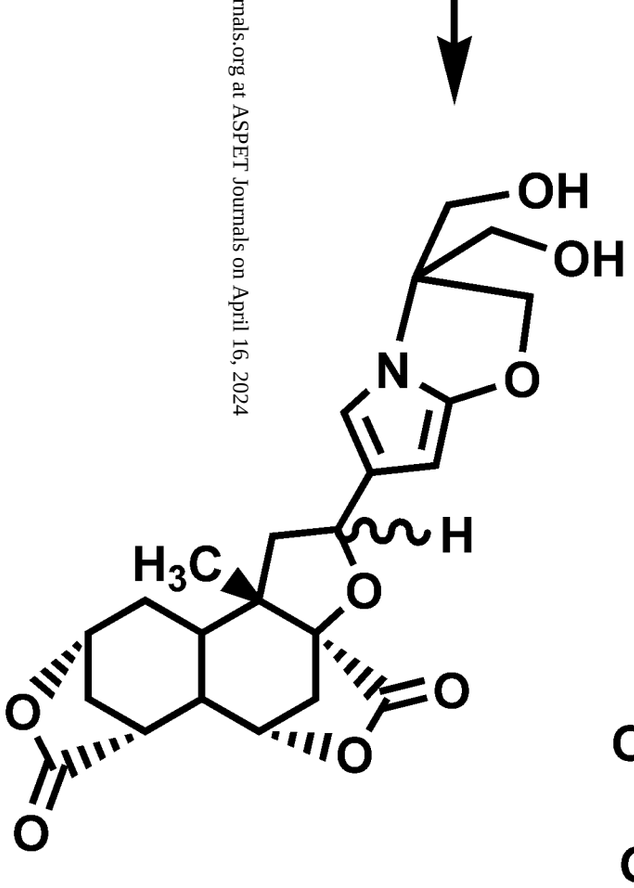

M7-M9

FIG 3

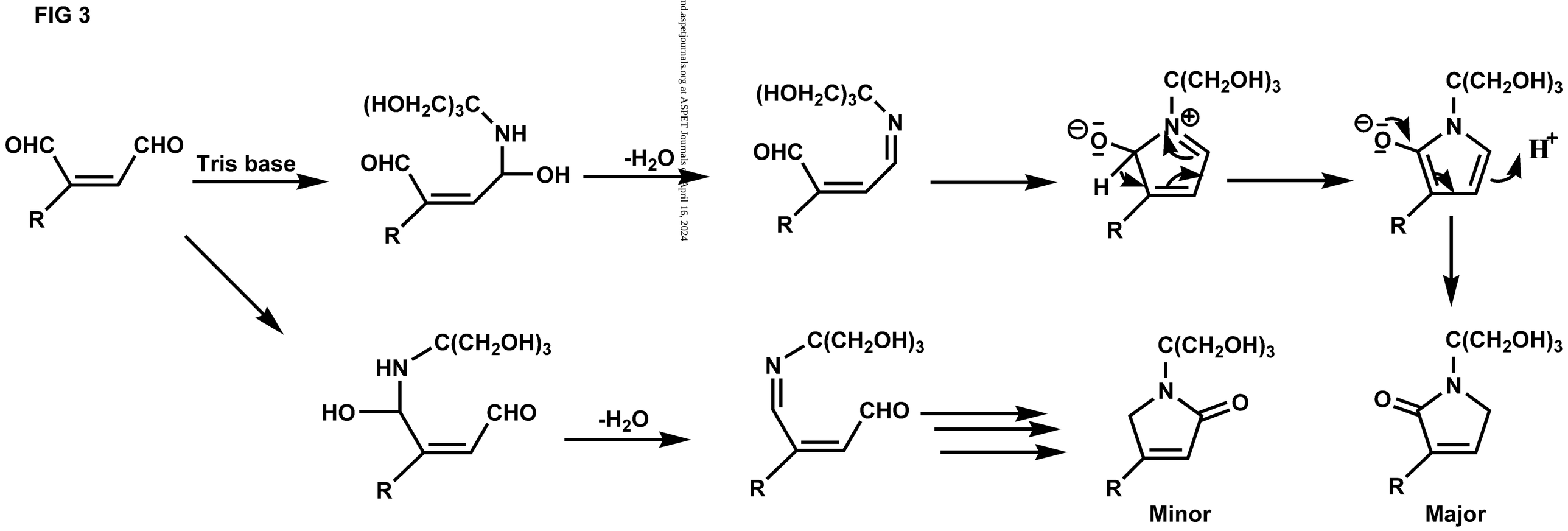

FIG 4

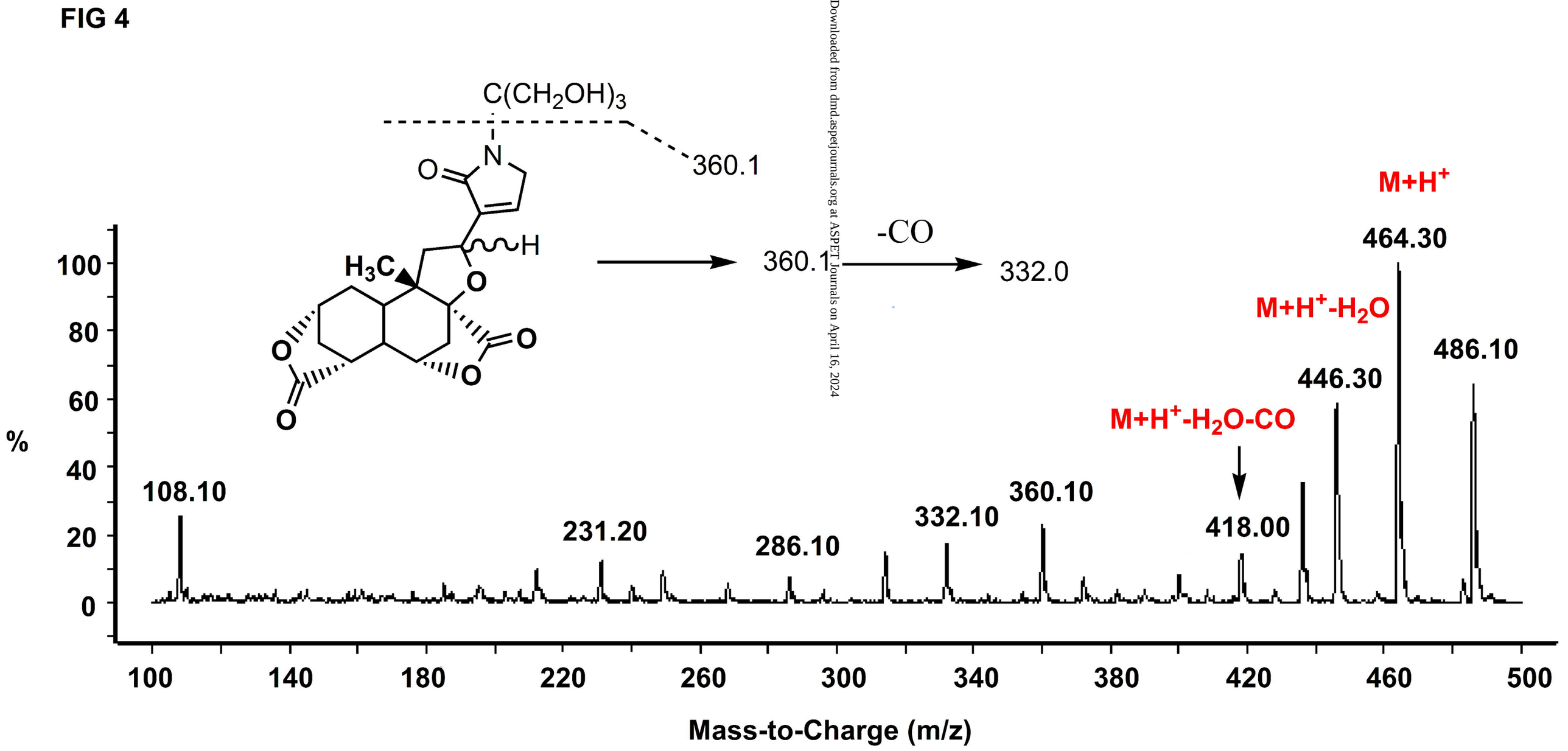

FIG 5

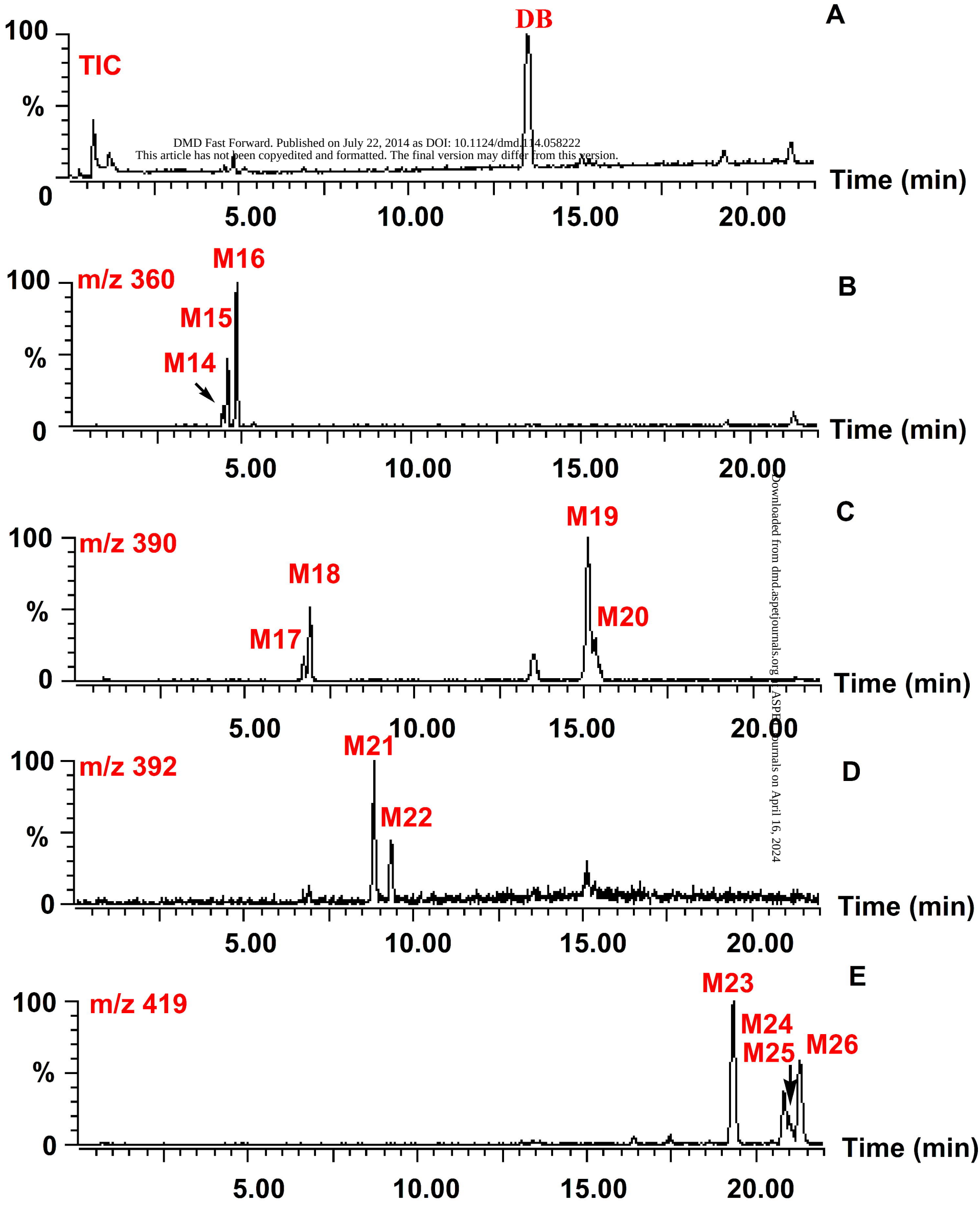

DMD Fast Forward. Published on July 22, 2014 as DOI: 10.1124/dmd.114.058222
This article has not been copyedited and formatted. The final version may differ from this version.

FIG 6

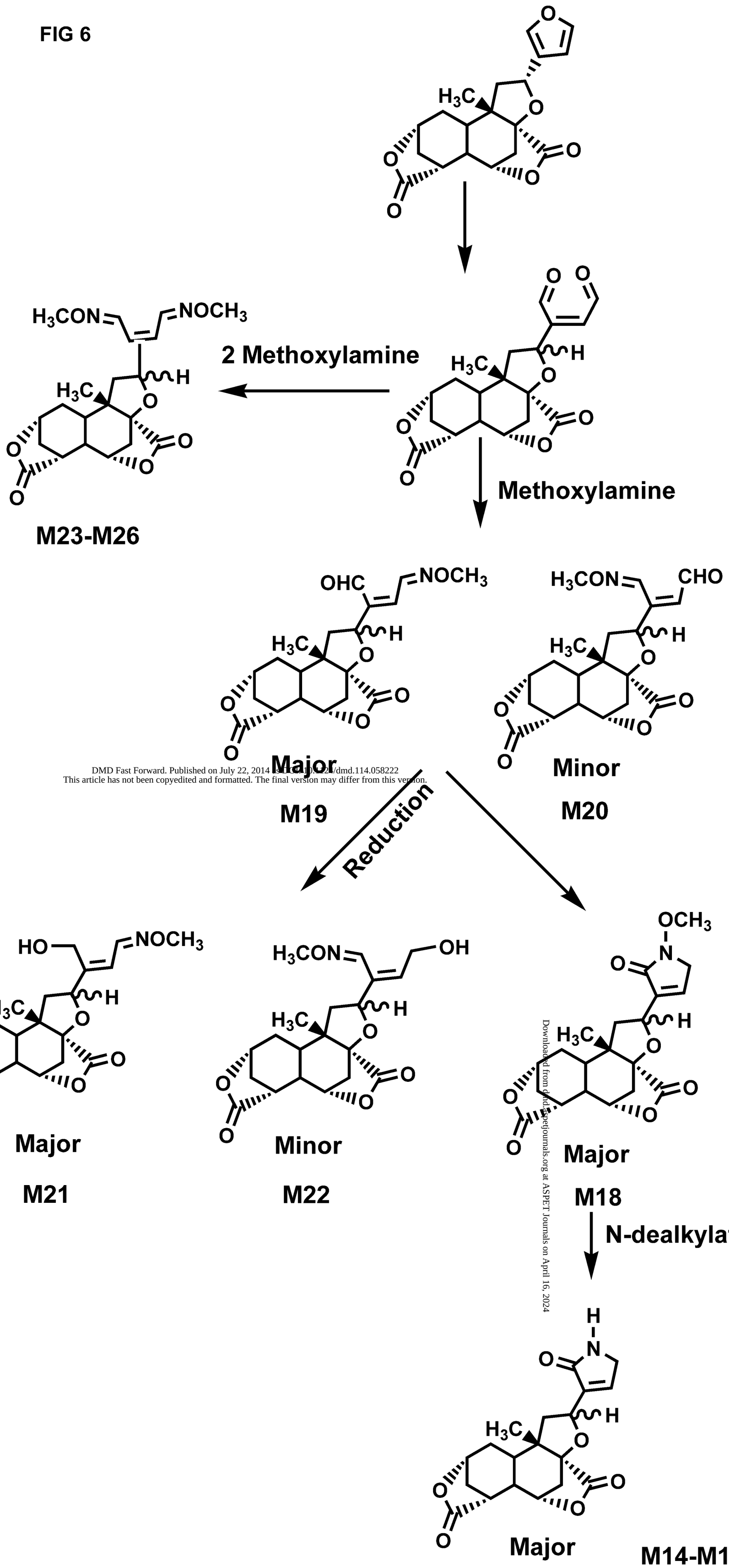

DMD Fast Forward. Published on July 22, 2014 as DOI: 10.1124/dmd.114.058222
This article has not been copyedited and formatted. The final version may differ from this version.

FIG 7

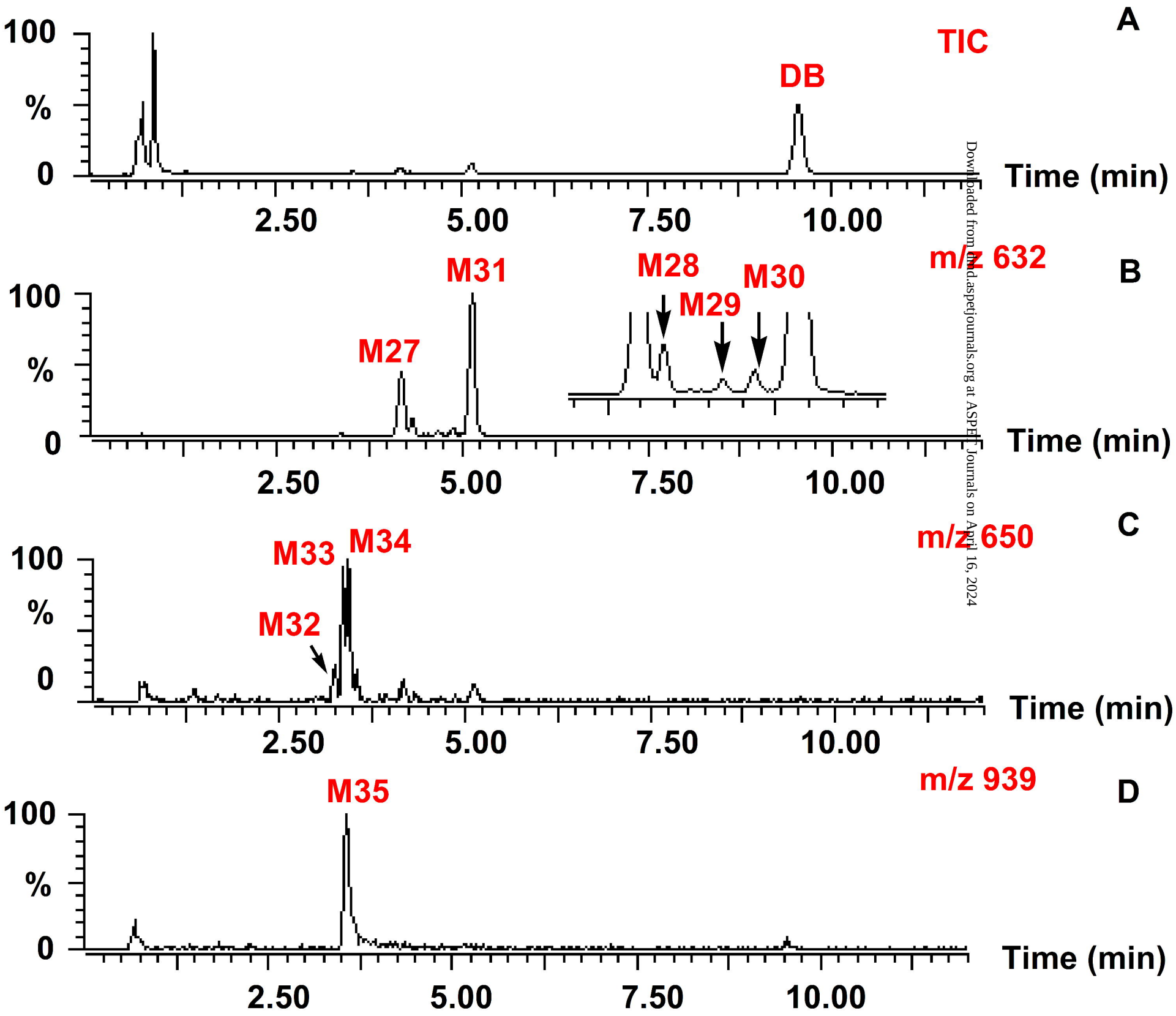

FIG 8

FIG 9

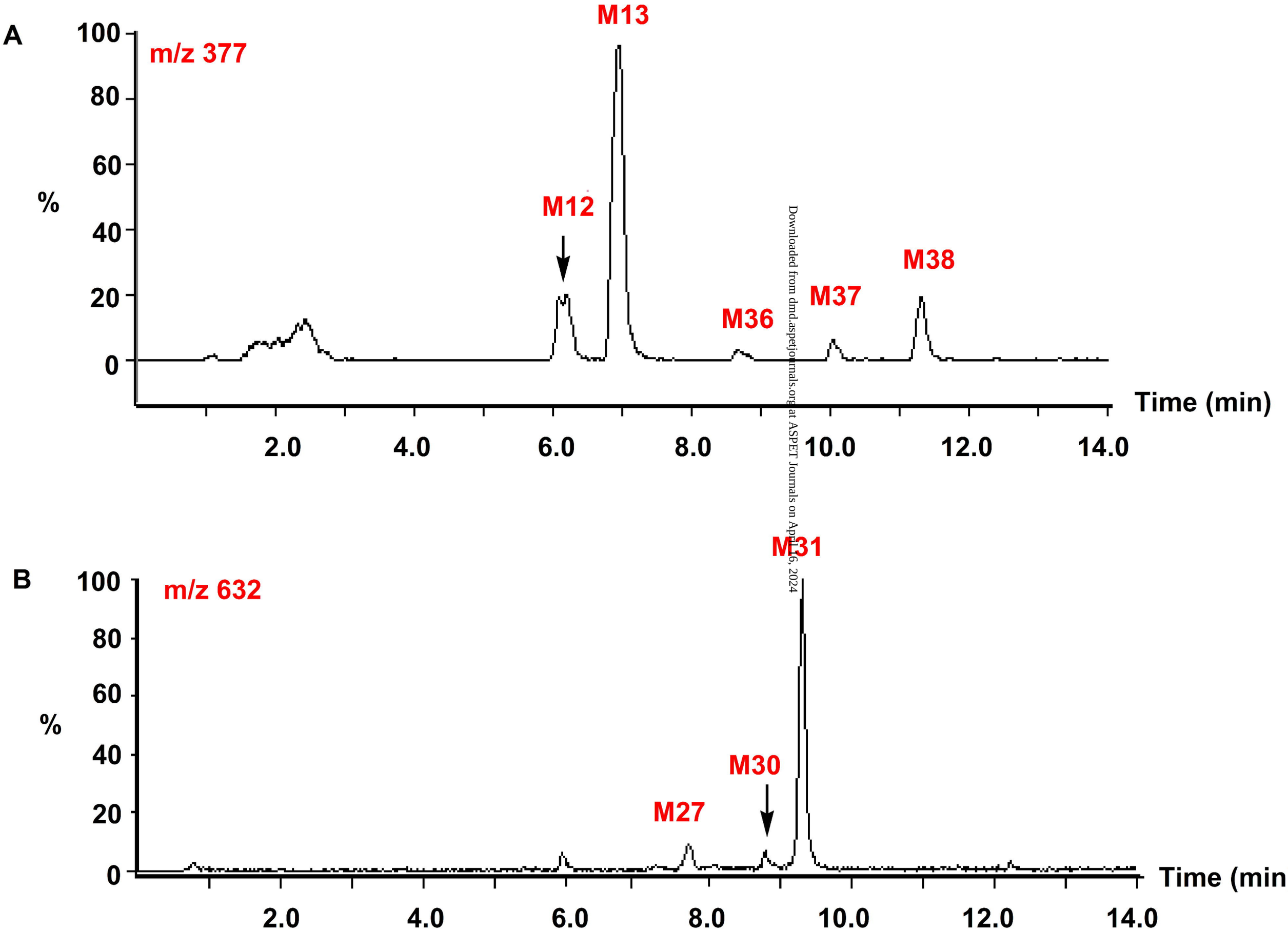

FIG 10

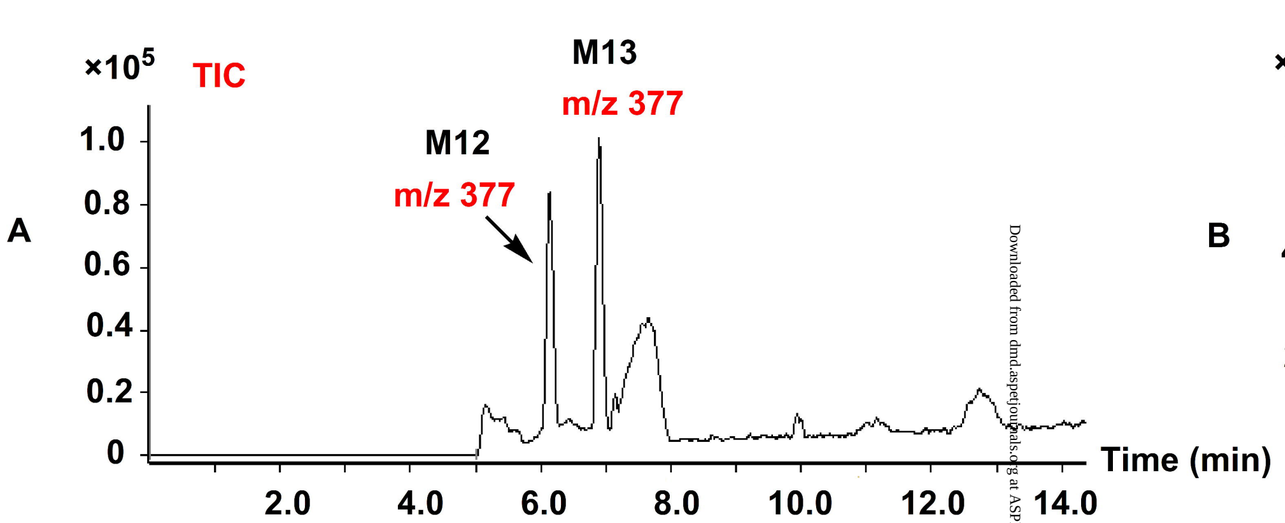

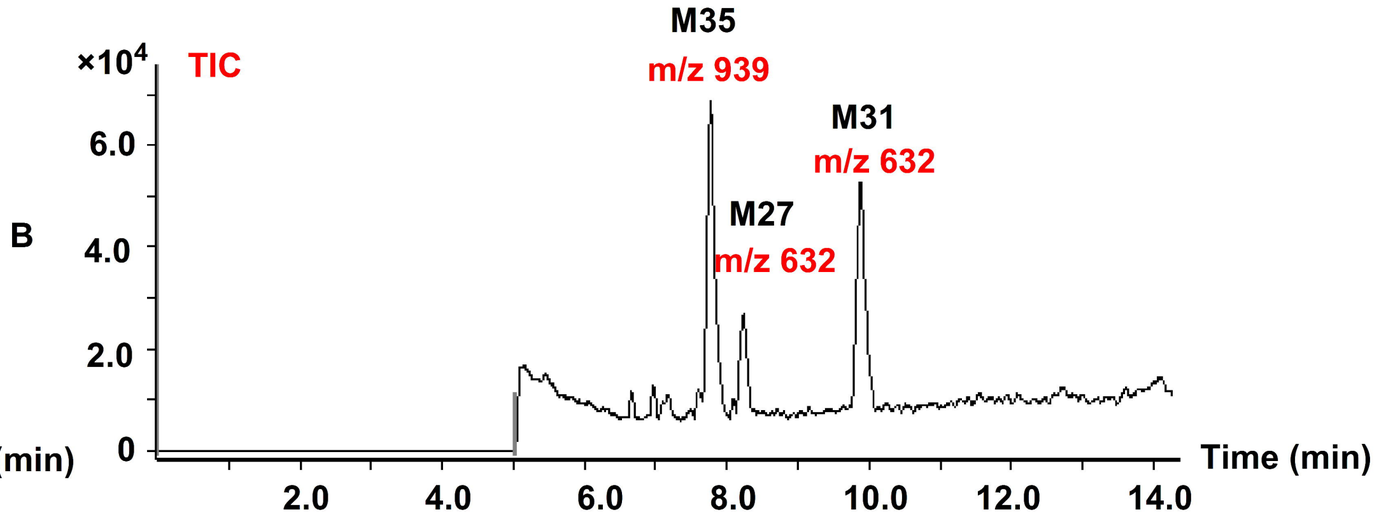

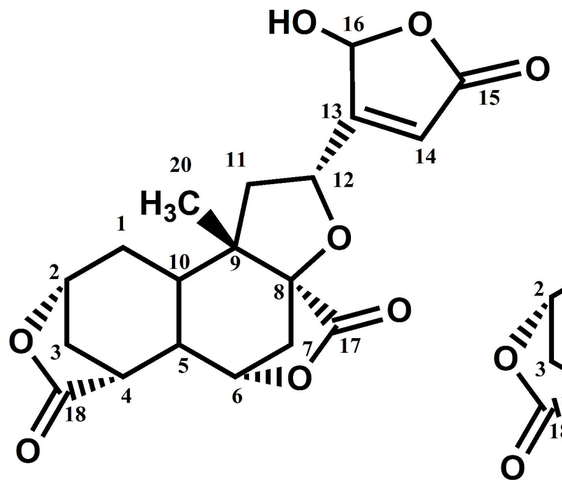

M12a (16 R), M12b (16 S)

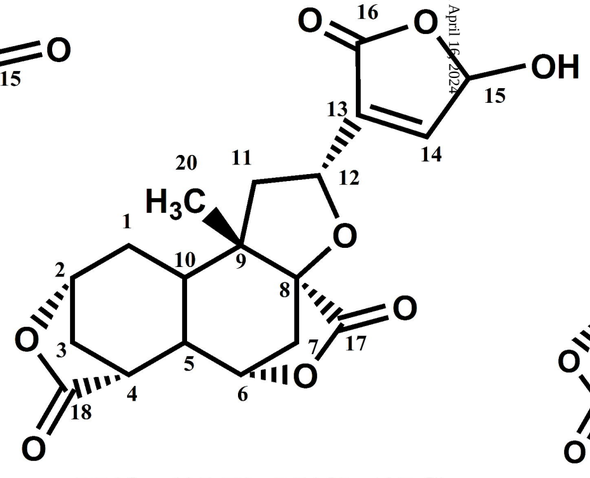

M13a (15 R), M13b (15 S)

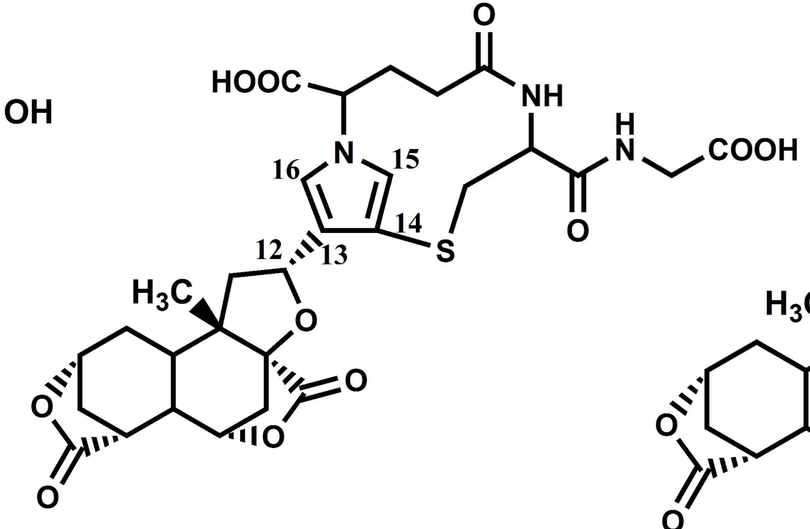

M31a

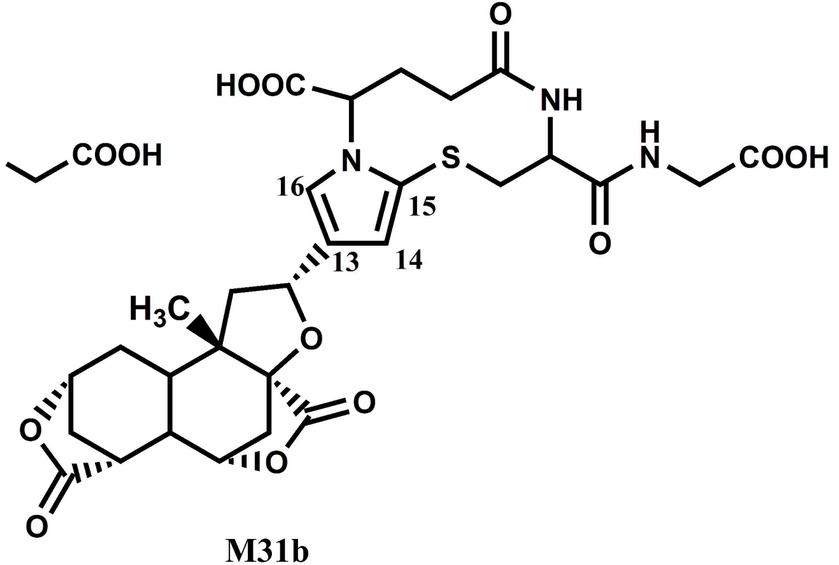

M31b

FIG 11

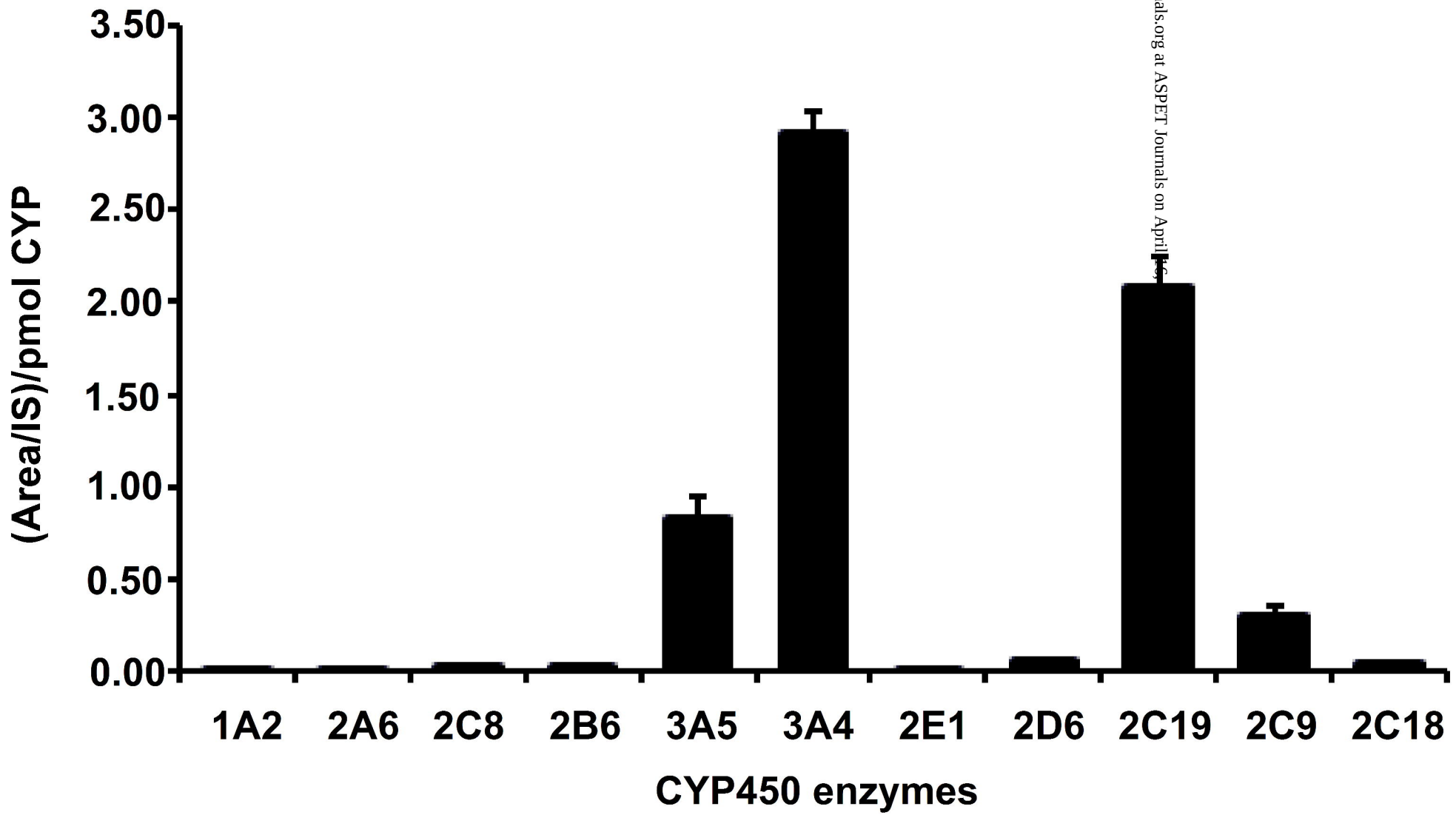

FIG 12

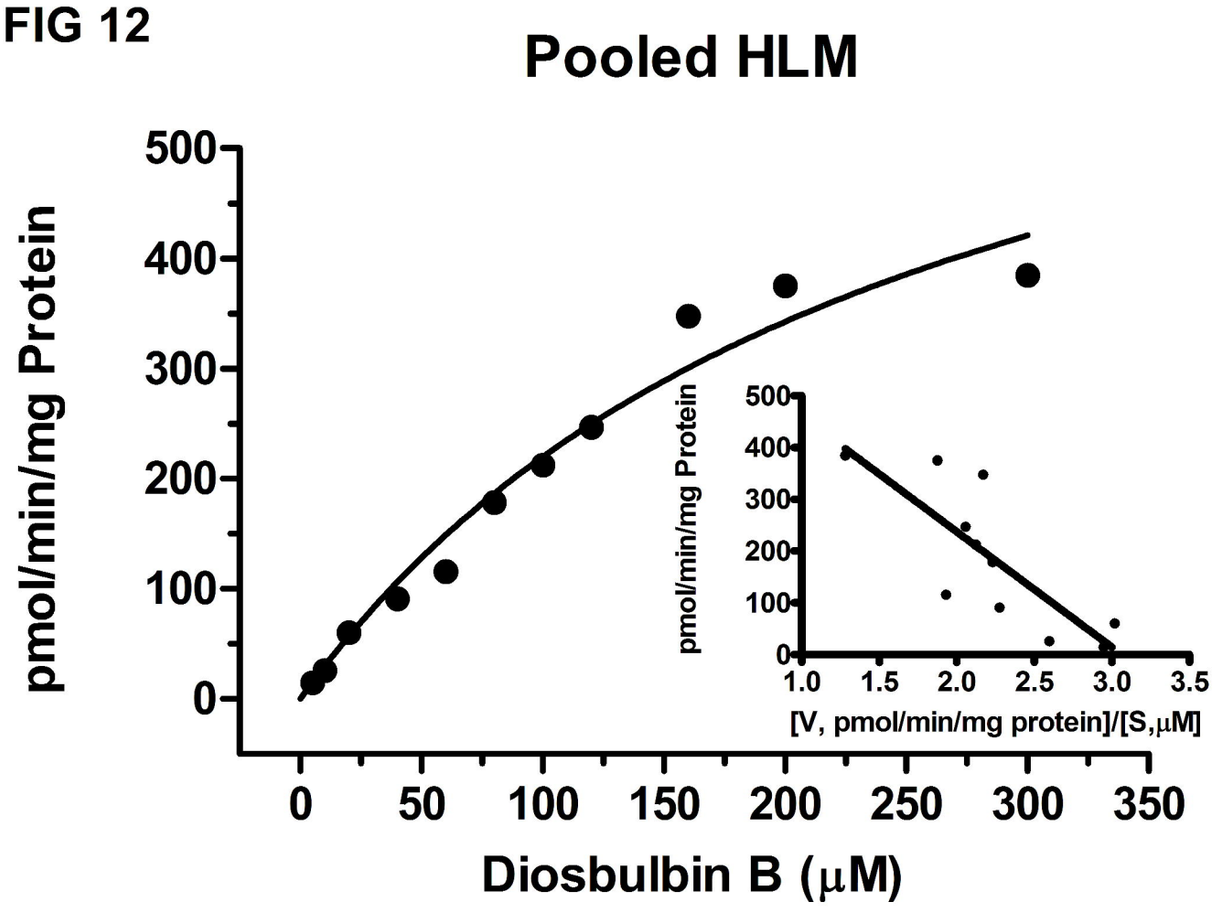

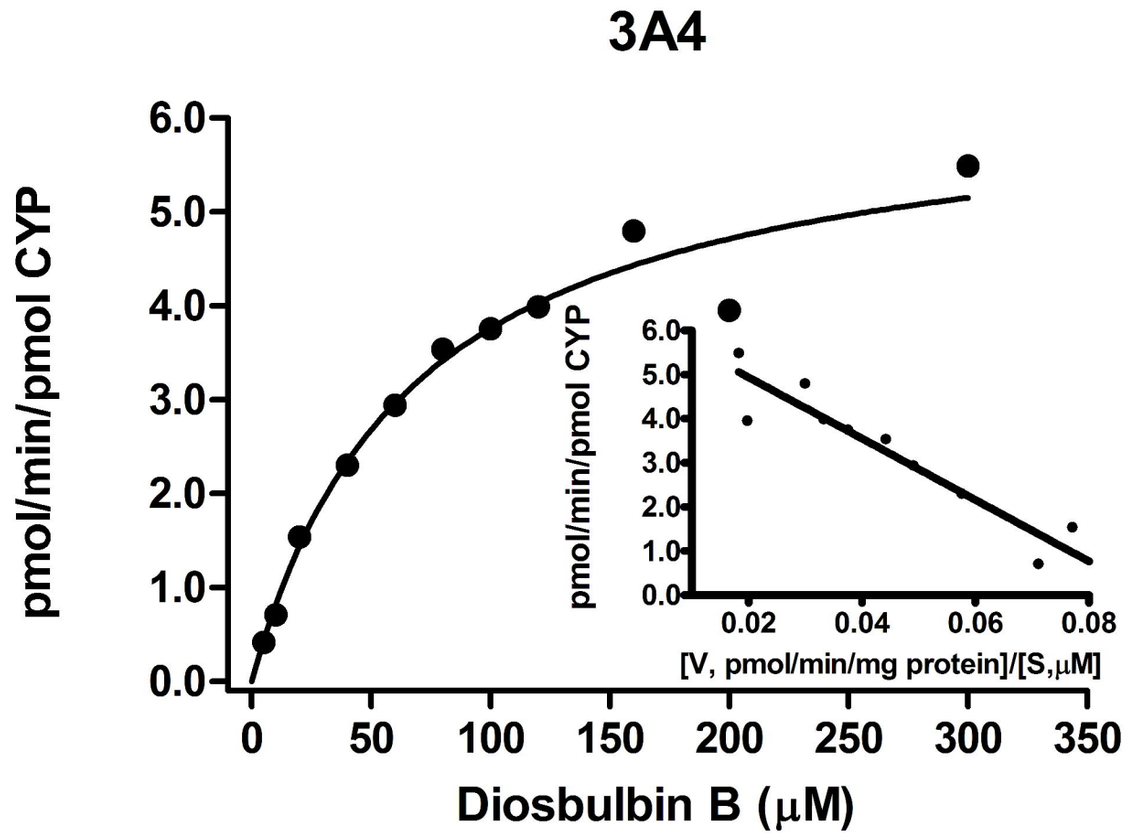

DMD Fast Forward. Published on July 22, 2014 as DOI: 10.1124/dmd.114.058222
This article has not been copyedited and formatted. The final version may differ from this version.